THESIS FOR THE DEGREE OF DOCTOR OF PHILOSOPHY

Multiscale methods for evolution problems

PER LJUNG

CHALMERS
UNIVERSITY OF TECHNOLOGY

UNIVERSITY OF GOTHENBURG

Division of Applied Mathematics and Statistics
Department of Mathematical Sciences
Chalmers University of Technology and University of Gothenburg
Gothenburg, Sweden 2023

Multiscale methods for evolution problems
Per Ljung
ISBN: 978-91-7905-842-5

Doktorsavhandlingar vid Chalmers tekniska högskola
Ny serie nr 5308
ISSN: 0346-718X

Division of Applied Mathematics and Statistics
Department of Mathematical Sciences
Chalmers University of Technology and University of Gothenburg
SE-412 96 Gothenburg, Sweden.
Phone: +46 (0)31 772 1000

Author e-mail: perlj@chalmers.se

Cover: The space-time decay of a basis correction for a multiscale parabolic equation where the diffusion contains high variations in both space and time (see Paper II).

Typeset with LaTeX
Printed in Gothenburg, Sweden 2023

Multiscale methods for evolution problems

Per Ljung

Division of Applied Mathematics and Statistics
Department of Mathematical Sciences
Chalmers University of Technology and University of Gothenburg

Abstract

In this thesis we develop and analyze generalized finite element methods for time-dependent partial differential equations (PDEs). The focus lies on equations with rapidly varying coefficients, for which the classical finite element method is insufficient, as it requires a mesh fine enough to resolve the data. The framework for the novel methods are based on the localized orthogonal decomposition (LOD) technique, introduced in [51]. The main idea of this method is to construct a modified finite element space whose basis functions contain information about the variations in the coefficients, hence yielding better approximation properties.

At first, the localized orthogonal decomposition framework is extended to the strongly damped wave equation, where two different highly varying coefficients are present (Paper I). The dependency of the solution on the different coefficients vary with time, which the proposed method accounts for automatically. Then we consider a parabolic equation where the diffusion is rapidly varying in both time and space (Paper II). Here, the framework is extended so that the modified finite element space uses space-time basis functions that contain the information of the diffusion coefficient. Furthermore, we study wave propagation problems posed on spatial networks (Paper III). Such systems are characterized by a matrix with large variations inherited from the underlying network. For this purpose, an LOD based approach adapted to general matrix systems is considered. Finally, we analyze the framework for a parabolic stochastic PDE with multiscale characteristics (Paper IV). In all papers we prove error estimates for the methods, and confirm the theoretical findings with numerical examples.

Keywords: Strongly damped wave equation, multiscale, localized orthogonal decomposition, finite element method, parabolic equations, spatial network models, stochastic partial differential equations.

List of appended papers

Paper I Per Ljung, Axel Målqvist, and Anna Persson: *A generalized finite element method for the strongly damped wave equation with rapidly varying data*. ESAIM Math. Model. Numer. Anal., 55(4):1375–1403, 2021.

Paper II Per Ljung, Roland Maier, and Axel Målqvist: *A space-time multiscale method for parabolic problems*. SIAM Multiscale Model. Simul., 20(2):714-740, 2022.

Paper III Morgan Görtz, Per Ljung, and Axel Målqvist: *Multiscale methods for solving wave equations on spatial networks*. Comput. Methods Appl. Mech. Eng., 410:116008, 2023.

Paper IV Annika Lang, Per Ljung, and Axel Målqvist: *Localized orthogonal decomposition for a multiscale parabolic stochastic partial differential equation*. (Submitted).

Contributions

Paper I The author of this thesis had the main responsibility to write and prepare the manuscript, took part in the analysis, and made the implementation for the numerical examples. The ideas were developed in close collaboration between the authors.

Paper II The ideas were developed as a collaboration between all authors. The authors of this thesis had the main responsibility of implementation for the numerical examples, and the responsibility of writing and preparing the manuscript was shared with Roland Maier.

Paper III The author of this thesis had the main responsibility of writing and preparing the manuscript, performed the error analysis and developed the ideas in collaboration with the other authors.

Paper IV The author of this thesis developed the ideas, performed the error analysis, made the implementation for the numerical examples and had the main responsibility of writing and preparing the manuscript. Annika Lang and Axel Målqvist provided valuable input throughout.

Acknowledgements

First of all, I wish to express my gratitude to my supervisor Axel Målqvist for his fantastic guidance and support throughout the work of this thesis. Your expertise and positivity have been invaluable to me these last few years. I would also like to thank my co-authors Anna Persson, Roland Maier, Morgan Görtz, and Annika Lang. I have learnt so much from all of you about the academic world, and about mathematics in general. I am truly lucky to have had the luxury of working with all of you.

Furthermore, I want to thank my colleagues at the department, especially those in the CAM group, for providing such a friendly work environment. In particular, thanks to Gustav Lindwall for always letting me knock on your door and helping me with all sorts of work related things, and for our many coffee break strolls.

At last, I want to thank my many close friends for all online and offline activities we have shared over the last few years. Especially, thanks to Therese for your constant love and support, and for always lifting my spirits.

Contents

Abstract iii

List of publications v

Acknowledgements vii

Contents ix

1 Introduction 1

2 The finite element method 3

2.1 Stationary equations 3

2.2 Evolution problems 6

2.3 Stochastic PDEs 12

3 Localized orthogonal decomposition (LOD) 19

3.1 LOD in the elliptic setting 19

3.2 LOD for time-dependent problems 27

4 LOD for evolution problems 29

4.1 Strongly damped wave equation 30

4.2 Parabolic equation with time-dependent diffusion 38

4.3 Wave equation on spatial networks 47

4.4 Parabolic SPDE with additive noise 56

5 Summary of papers **67**

Bibliography **69**

Papers I-IV

1 Introduction

The modeling of partial differential equations (PDEs) is a major topic in both science and engineering. Applications range from simulating the aerodynamics of large aircraft to the modeling of atoms on a quantum mechanic level. In this thesis, we focus on time-dependent partial differential equations. In particular, we are interested in simulations of strongly heterogeneous materials, such as, e.g., composite materials. The modeling of such materials result in PDEs with highly oscillatory coefficients. This type of problems, where the data is varying rapidly, is referred to as *multiscale problems*.

One of the most common numerical approaches to solving PDEs is the finite element method (FEM). However, for multiscale problems, FEM approximations are only accurate if the mesh is fine enough to resolve the variations in the data. This quickly becomes challenging in terms of computational cost and memory. For the purpose of solving multiscale equations, several so-called *multiscale methods* have been developed. Some of these methods are inspired by analytical homogenization theory, such as the heterogeneous multiscale method (HMM) [16, 1] and the multiscale finite element method [29]. In order to prove convergence, these methods require strong assumptions on periodicity and scale separation. In addition, several multiscale methods have been developed that circumvent these sorts of requirements. Examples of such methods include generalized (multiscale) finite element methods [7, 6, 18] and gamblets [56, 57]. In particular, this thesis is mainly based on the framework of a generalized finite element method (GFEM) known as the localized orthogonal decomposition (LOD) method, first introduced in [51].

The LOD method is based on the variational multiscale method (VMS) [30, 41, 48, 40]. The main idea of the method is to construct a modified coarse-scale finite element space enriched by problem-dependent fine-scale correctors. In turn, it was proven in [51] (and later improved in [28]) that these correctors satisfy an exponential decay, making it possible to restrict the computations to local patches, which is one of the advantages of the LOD method. Another

strength is that the correctors are completely independent and can be computed in parallel. In [51], convergence of optimal order is proven independent of the variations in the data, with no assumptions made on neither periodicity nor scale separation. The LOD method was first introduced for elliptic equations, but has since then been further developed and analyzed for several types of problems, including time-dependent PDEs such as parabolic ones in [49, 50, 3] and wave-type equations in [2, 47]. For more results on the LOD method, see, e.g., [27, 26, 52, 54, 25], and for a general and rigorous introduction to the topic, we refer to [53].

The purpose of this thesis is to extend the LOD framework to evolution problems. In a broad sense, this is done in two ways. In Papers I-II, we consider equations where the time-dependency has to be taken into account in the construction of the multiscale method, whereas Papers III-IV apply the well-established stationary LOD method to new types of settings. For all works, we derive a priori error analysis, and illustrate the results with numerical examples. In summary, the thesis consists of the following works.

Paper I. We derive an LOD method for the so-called *strongly damped wave equation*. This case is unique as the PDE consists of two different multiscale coefficients, while multiscale methods such as LOD are in general designed to handle only one coefficient.

Paper II. A parabolic problem where the diffusion varies rapidly in both space and time is considered. For this, a space-time multiscale method based on the variational multiscale method and the LOD method is presented and analyzed.

Paper III. We consider wave propagation problems posed on so-called spatial networks. Such problems are characterized by a symmetric, positive-definite matrix K, whose data contain high variations inherited from the network structure. These variations are dealt with by defining an LOD based method for general matrix systems.

Paper IV. The LOD method is presented and analyzed for a parabolic stochastic partial differential equation. The method shows further promise when applied together with (multilevel) Monte-Carlo estimation, where an extensive number of solutions has to be computed.

Outline: In Chapter 2 we present the classical finite element method and illustrate why it is not sufficient for problems where the data is highly varying. Chapter 3 introduces the LOD method for elliptic equations, and its extension to evolution problems. Finally, Chapter 4 presents the methods and summarizes the main results from Papers I-IV.

2 The finite element method

In this chapter we present the finite element method and discuss why it becomes computationally expensive to use for problems with highly oscillatory data. At first, we define the method for elliptic equations, and illustrate both theoretically and numerically how the high data variations affect the convergence rate. Subsequently, we present the finite element method in the context of evolution problems, and discuss the characteristics of the continuous solutions as well as their approximated counterparts.

2.1 Stationary equations

Consider the elliptic equation

$$\begin{aligned} -\nabla \cdot (A\nabla u) &= f, \text{ in } D, \\ u &= 0, \text{ on } \partial D, \end{aligned} \tag{2.1.1}$$

where $D \subset \mathbb{R}^d$, $d = 2, 3$ is a bounded Lipschitz-domain with polygonal boundary, $f \in L_2(D)$ is the source function, and $A = A(x) \in L_\infty(D, \mathbb{R}^{d\times d}_{\text{sym}})$ is the (highly oscillatory) diffusion coefficient that satisfies

$$0 < \alpha_- := \operatorname*{ess\,inf}_{x\in D} \inf_{v\in\mathbb{R}^d\setminus\{0\}} \frac{A(x)v\cdot v}{v\cdot v} \leq \operatorname*{ess\,sup}_{x\in D} \sup_{v\in\mathbb{R}^d\setminus\{0\}} \frac{A(x)v\cdot v}{v\cdot v} =: \alpha_+ < \infty.$$

We begin by introducing the standard Sobolev spaces used in finite element theory. Let $\alpha = (\alpha_1, \dots \alpha_d)$ be a multi-index, and define

$$\mathrm{D}^\alpha \varphi := \frac{\partial^{|\alpha|}\varphi}{\partial x_1^{\alpha_1} \cdots \partial x_d^{\alpha_d}},$$

where $|\alpha| := \alpha_1 + \ldots + \alpha_d$. We say that v is the *α'th order weak derivative of u* if for all $\varphi \in C_0^{|\alpha|}(D)$ it holds

$$\int_D u \mathrm{D}^\alpha \varphi \,\mathrm{d}x = (-1)^{|\alpha|} \int_D v\varphi \,\mathrm{d}x,$$

where $C_0^{|\alpha|}(D)$ is the space of $|\alpha|$ times continuously differentiable functions with compact support in D. If the linear functional $\mathrm{D}^\alpha\varphi$ is bounded in $L_2(D)$, we identify it with an element $\mathrm{D}^\alpha v \in L^2(D)$ using the same notation. With the weak derivative defined, we may construct the Sobolev space $H^k(D)$ for $k \geq 0$ as the space of all functions whose weak derivatives of order smaller than or equal to k belong to $L_2(D)$, i.e.,

$$H^k(D) := \{v \in L_2(D) \colon \mathrm{D}^\alpha v \in L_2(D) \text{ for } |\alpha| \leq k\},$$

equipped with inner product and corresponding norm

$$\begin{aligned}(v, w)_{H^k} &:= \sum_{|\alpha|\leq k} \int_D \mathrm{D}^\alpha v \mathrm{D}^\alpha w \,\mathrm{d}x,\\ \|v\|_k^2 := (v, v)_{H^k} &= \sum_{|\alpha|\leq k} \int_D (\mathrm{D}^\alpha v)^2 \,\mathrm{d}x.\end{aligned}$$

We moreover define the corresponding seminorm on $H^k(D)$ as

$$|v|_k^2 := \sum_{|\alpha|=k} \int_D (\mathrm{D}^\alpha v)^2 \,\mathrm{d}x.$$

In particular, we introduce $H_0^1(D)$ as the classical Sobolev space with norm

$$\|v\|_{H^1(D)}^2 := \|v\|_{L_2(D)}^2 + \|\nabla v\|_{L_2(D)}^2$$

with functions vanishing on ∂D in the sense of traces. In the following, we abbreviate the $L_2(D)$-norm as $\|\cdot\| := \|\cdot\|_{L_2(D)}$.

We derive the weak formulation corresponding to (2.1.1), on which we base our finite element method. By standard procedure we multiply the equation by a test function $v \in H_0^1(D)$ and integrate by parts over the domain D. The weak formulation becomes: find $u \in H_0^1(D)$ such that

$$a(u, v) = (f, v), \tag{2.1.2}$$

for all $v \in H_0^1(D)$, where $(\cdot, \cdot)$ is the standard $L_2(D)$-scalar product and $a(\cdot, \cdot) := (A\nabla\cdot, \nabla\cdot)$. We wish to define a FEM for the problem by constructing

a discretized version of the weak formulation (2.1.2). To this end, let $\{\mathcal{T}_h\}_{h>0}$ denote a family of shape regular triangulations that form a partition of the domain D. For an element $T \in \mathcal{T}_h$ we define the corresponding mesh size as $h_T := \text{diam}(T)$, and denote the largest diameter by $h := \max_{T\in\mathcal{T}_h} h_T$. Next, we construct the classical finite element space using continuous piecewise linear polynomials

$$S_h := \big\{v \in C(\bar{D}) : \ v\big|_T \text{ is a polynomial of partial degree} \leq 1, \forall T \in \mathcal{T}_h\big\},$$

and let $V_h := S_h \cap H_0^1$. The finite element formulation now follows by considering a Galerkin ansatz based on the discretized space V_h. More precisely: find $u_h \in V_h$ such that

$$a(u_h, v) = (f, v), \tag{2.1.3}$$

holds for all $v \in V_h$.

From a computational point of view, the system (2.1.3) is regarded as a linear matrix system. To be precise, denote by $\mathcal{N}_h$ the set of interior nodes in $\mathcal{T}_h$ with cardinality $|\mathcal{N}_h| = N_h$, and $\{\varphi_i\}_{i=1}^{N_h}$ the set of piecewise linear basis functions that spans V_h. Then, we can express $u_h = \sum_{i=1}^{N_h} \alpha_i\varphi_i$, insert this into (2.1.3) and test with basis functions $v = \varphi_j$, $j = 1, \ldots, N_h$. This results in an $N_h \times N_h$ matrix system

$$K\hat{u} = M\hat{f}, \tag{2.1.4}$$

where $K_{ij} = a(\varphi_j, \varphi_i)$, $(M\hat{f})_j = (f, \varphi_j)$, and $\hat{u}_i = \alpha_i$. In Section 3.1, we return to a discussion on general matrix systems of the kind (2.1.4), where K contains high data variations. This topic is central in the work of Paper III.

From standard a priori error analysis (see, e.g., [42, Theorem 5.1]), the following error bound is derived for the finite element approximations in (2.1.3)

$$\|u_h - u\|_{H^1(D)} \leq Ch\|u\|_{H^2(D)}.$$

This convergence result is valid for $u \in H^2(D)$, which is satisfied under the assumption $A \in C^1(D)$ for a convex domain D. Assume for the moment that A is a scalar valued coefficient. The H^2-seminorm can further be bounded as

$$\begin{aligned} |u|_2 &\leq C\|\Delta u\| \leq C\|A\nabla\cdot(\nabla u)\| = C\|\nabla\cdot(A\nabla u) - \nabla A\nabla u\| \\ &\leq C\|\nabla\cdot(A\nabla u)\| + \|\nabla A\|_{L_\infty}\|\nabla u\| \leq C(1 + \|\nabla A\|_{L_\infty})\|f\| \end{aligned}$$

where the first inequality follows from elliptic regularity and the last inequality from $\|u\|_{H^1(D)} \leq C\|f\|$, which can be derived from the weak formulation. Note

here that the error is bounded by the derivative of the diffusion A. Hence, if A is rapidly varying with frequency ε^{-1}, then $\|\nabla A\|_{L_\infty} = \mathcal{O}(\varepsilon^{-1})$. Consequently, the error of the FEM approximation has the upper bound

$$\|u_h - u\|_{H^1(D)} \leq C \min\{h + h\varepsilon^{-1}, 1\}\|f\|.$$

In practice, this means that the sought convergence rate may not be achieved unless $h < \varepsilon$. As ε gets smaller, i.e., the diffusion varies more rapidly, this condition quickly becomes difficult to satisfy in terms of computational complexity and memory.

To demonstrate this phenomenon, we present a numerical example. We set the domain to be the unit square, i.e., $D = [0, 1] \times [0, 1]$, and let the diffusion coefficient be given by

$$A(x_1, x_2) = 102 + 100 \sin\left(\frac{2\pi x_1}{\varepsilon}\right) \sin\left(\frac{2\pi x_2}{\varepsilon}\right), \tag{2.1.5}$$

where ε denotes the scale at which the diffusion varies. An example of this coefficient when $\varepsilon = 2^{-4}$ is seen in Figure 2.1b. We compute a reference solution, denoted u_{ref}, on a fine mesh with mesh size $h = 2^{-8}$, and compute the error between the reference solution u_{ref} and finite element approximation u_h for $h = 2^{-1}, 2^{-2}, \ldots, 2^{-7}$. The error is measured in the energy norm, defined by

$$|||\cdot||| := \sqrt{a(\cdot, \cdot)}.$$

This is done for different choices of $\varepsilon = 2^{-1}, 2^{-2}, \ldots, 2^{-5}$. The convergence plots are seen in Figure 2.1a. Here we can see how the error remains on a constant level until the mesh is able to resolve the variations defined by ε, at which point we start to see the linear convergence rate.

2.2 Evolution problems

We continue the discussion on the finite element method by introducing some common time-dependent equations, and present their main characteristics and approximation results. At first, we consider parabolic-type equations, which is the particular focus in Paper II and Paper IV. Subsequently, we introduce the wave-type equations which are examined in Paper I and Paper III, respectively.

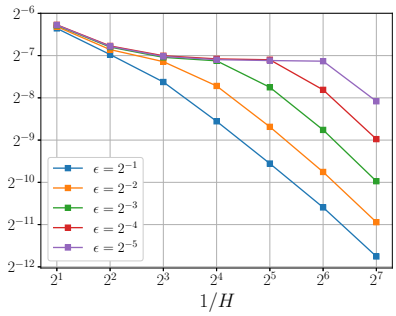

(a) Energy error.

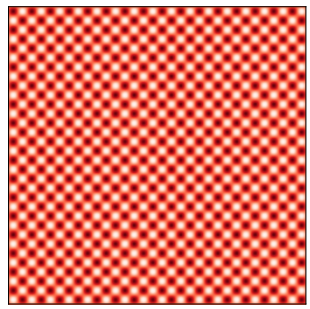

(b) $A(x_1, x_2)$.

Figure 2.1: The left image shows the energy error $|||u_h - u_{\text{ref}}|||$ as function of mesh size for different choices of scale ε. The right image is the coefficient used in the case $\varepsilon = 2^{-4}$.

Parabolic equation

Consider the parabolic equation

$$\begin{aligned} \dot{u} - \nabla \cdot (A \nabla u) &= f, \quad \text{in } D \times (0, T], \\ u &= 0, \quad \text{on } \partial D \times (0, T], \\ u(0) &= u_0, \quad \text{in } D, \end{aligned} \tag{2.2.1}$$

where the domain D and the diffusion A are defined as in Section 2.1, $f = f(t, x)$ is a time-dependent source function, $u_0 \in L_2(D)$ is the initial value of the system, and $T > 0$ is the final time. For now, we still assume $A = A(x)$ to be independent of time. Later, in Paper II, the system (2.2.1) is considered with $A = A(t, x)$ rapidly varying in both space and time.

Following the standard procedure applied in the previous section, the variational formulation corresponding to (2.2.1) reads: find $u(t, \cdot) \in H_0^1(D)$ with $u(0, \cdot) = u_0$, such that for all $v \in H_0^1(D)$, it holds

$$(\dot{u}, v) + a(u, v) = (f, v). \tag{2.2.2}$$

We proceed by stating some important characteristics of the solution to (2.2.2). At first, we recall *Duhamel's principle* (see, e.g., [64, Chapter 1]), stating that the

solution to (2.2.2) is given by

$$u(t) = E(t)u_0 + \int_0^t E(t-s)f(s)\,\mathrm{d}s,$$

where $E(t)$ is the solution operator to the homogeneous case, i.e., when $f \equiv 0$. The operator $E(t)$ can also be seen as the semigroup generated by the diffusion operator $-\nabla \cdot A\nabla$, and is commonly used in a priori analysis for parabolic equations. In particular, Duhamel's principle and properties of the solution operator $E(t)$ are both central in the error analysis presented in Paper IV.

For evolution equations, the total energy of the solution is bounded by the source and initial data. More precisely, by Duhamel's principle and the stability of $E(t)$ in $L_2(D)$-norm (see, e.g., [42, 64]), it follows immediately that

$$\|u(t)\| \leq \|u_0\| + \int_0^t \|f(s)\|\,\mathrm{d}s.$$

We note that in the homogeneous case, the total energy of the system is bounded by the size of the initial value. In fact, if we let λ_1 be the first eigenvalue of the diffusion operator $-\nabla \cdot A\nabla$, one can further show that the solution u satisfies the exponential decay

$$\|u(t)\| \leq e^{-\lambda_1 t}\|u_0\|, \quad t \geq 0, \tag{2.2.3}$$

in the absence of a source function. This exponential decay is a natural property for parabolic problems. In both Paper I and Paper II, the decay property is exploited in order to improve the computational efficiency of the corresponding presented numerical methods.

We continue by deriving the finite element method for (2.2.2). In similarity to the previous section, we replace the solution space $H_0^1(D)$ by the finite element space V_h. This yields a spatially discretized version of (2.2.2), referred to as the *semi-discrete Galerkin method*. It reads: find $u_h(t) \in V_h$ such that

$$(\dot{u}_h, v) + a(u_h, v) = (f, v), \tag{2.2.4}$$

for all $v \in V_h$ with initial value $u_h(0) = u_{0,h}$, where $u_{0,h} \in V_h$ is some convenient approximation of u_0, e.g., the $L_2(D)$-projection onto V_h.

In contrast to the stationary equations, evolution problems are moreover defined on the temporal domain $[0, T]$, for which we require further discretization. For this purpose, let $0 =: t_0 < t_1 < \ldots < t_N := T$ be a uniform partition with time step $\tau = t_n - t_{n-1}$. Here, we have chosen a uniform time step to simplify

the presentation, but remark that the results are easily extended to the case of varying time step. Now, let $u_h^n = u_h(t_n)$, and denote by $\bar{\partial}_t$ the (backwards) discrete time derivative defined as $\bar{\partial}_t u_h^n = (u_h^n - u_h^{n-1})/\tau$. The *backward Euler–Galerkin scheme* becomes: find $u_h^n \in V_h$ for $n = 1, \dots, N$, with initial value $u_h^0 = u_{0,h}$, such that

$$(\bar{\partial}_t u_h^n, v) + a(u_h^n, v) = (f^n, v), \tag{2.2.5}$$

holds for all $v \in V_h$.

From standard a priori analysis, it is well-known that the scheme (2.2.5) converges in $L_2(D)$-norm with second order in space, and first order in time (see, e.g., [42, Theorem 10.5]). However, in analogy with Section 2.1, the constant in the error bound depends on the scale ε on which the diffusion A varies. More precisely, the error estimate becomes

$$\|u_h^n - u(t_n)\| \leq C(\tau + h^2/\varepsilon).$$

That is, the sought convergence rate (in spatial sense) is not reached unless the mesh size satisfies $h < \varepsilon$. In Chapter 3, we discuss how to circumvent this issue by introducing multiscale approximation techniques.

Remark 2.2.1 (Choice of temporal scheme). In (2.2.5), the temporal scheme is represented by the backward Euler scheme. This choice is well-suited for parabolic equations, as it is unconditionally stable, i.e., it attains stable solutions regardless of the relation between mesh size h and time step τ. Another possibility is to apply a symmetric scheme to (2.2.4) known as the *Crank–Nicolson scheme*. Like backward Euler, Crank–Nicolson is an unconditionally stable time stepping scheme, but attains second order convergence rate in time due to its symmetry. In Paper I and Paper IV, the temporal discretizations are based on backward Euler, while Crank–Nicolson is applied in Paper II.

Wave equation

Consider the linear wave equation

$$\begin{aligned} \ddot{u} - \nabla \cdot (A \nabla u) &= f, \quad \text{in } D \times (0, T], \\ u &= 0, \quad \text{on } \partial D \times (0, T], \\ u(0) = u_0, \ \dot{u}(0) &= v_0, \quad \text{in } D, \end{aligned} \tag{2.2.6}$$

where D, A, f, u_0 are defined as in the parabolic equation (2.2.1), and v_0 is an additional initial value. Our goal is to derive characteristics of the solution to (2.2.6), and mention important differences from the previously considered

parabolic case.

Straight-forwardly, we have the semi-discrete Galerkin formulation to find $u_h(t) \in V_h$ such that

$$(\ddot{u}_h, v) + a(u_h, v) = (f, v), \tag{2.2.7}$$

holds for all $v \in V_h$, where the initial values $u_h(0) = u_{0,h}$ and $\dot{u}(0) = v_{0,h}$ are suitable approximations of u_0, v_0. An important property for the linear wave equation is its conservation of energy. Indeed, we have the following well-known result (see, e.g., [42, Lemma 13.1]).

Proposition 2.2.2 (Energy conservation)**.** *Let u_h be the solution to* (2.2.7) *with $f \equiv 0$. Then*

$$\|\dot{u}_h(t)\|^2 + |||u_h(t)|||^2 = \|v_{0,h}\|^2 + |||u_{0,h}|||^2, \quad t \geq 0. \tag{2.2.8}$$

The result states that (in the absence of external source) the total energy at time t remains the same as the initial energy. Note that this strictly differs from the parabolic case, in which the energy decays exponentially with time in the absence of source function f. We remark that the energy conservation is of importance when considering the choice of temporal discretization scheme for the wave equation. This is mainly due to some schemes, such as the backward Euler, causes so-called artificial *numerical damping*, and consequently yields inaccurate approximations for systems where the energy is conserved. For more details on the effect of artificial damping, we refer to the work in [10, 11].

For the temporal discretization of the wave equation, we deploy the scheme used in [42, Chapter 13]. That is, we seek $u_h^n \in V_h$ for $n = 2, \ldots, N$, with initial values $u_h^0, u_h^1 \in V_h$, such that

$$(\partial_t \bar{\partial}_t u_h^n, v) + a(\tfrac{1}{2}(u_h^{n+1/2} + u_h^{n-1/2}), v) = (f^n, v), \tag{2.2.9}$$

for all $v \in V_h$, where ∂_t and $\bar{\partial}_t$ denote the discrete forward and backward derivatives, respectively, and $u_h^{n+1/2} = (u_h^{n+1} + u_h^n)/2$. For this scheme, an analogous version of the stability estimate (2.2.8) is derived in [42, Lemma 13.2]. More precisely, when $f^n = 0$, it holds that

$$\|\partial_t u_h^n\|^2 + |||u_h^{n+1/2}|||^2 = \|\partial_t u_h^0\|^2 + |||u_h^{1/2}|||^2, \quad n \geq 0.$$

Following the standard a priori analysis for wave equations (see, e.g., [42, Theorem 13.2]), it holds that the approximation from (2.2.9) converges with optimal order in space, i.e., linearly in $H_0^1(D)$-norm and quadratically in $L_2(D)$.

Moreover, by the symmetrical scheme made in time, we get second order convergence in time as well. To be exact, the error satisfies

$$\|u_h^{n+1/2} - u(t_n + \tau/2)\| \leq C(\tau^2 + h^2/\varepsilon),$$
$$|||u_h^{n+1/2} - u(t_n + \tau/2)||| \leq C(\tau^2 + h/\varepsilon).$$

Once again, we have included the effect of ε, the scale at which the diffusion A oscillates, to emphasize the drawback of the standard finite element method in multiscale applications.

Strongly damped wave equation

We conclude the part on evolution problems by introducing the so-called *strongly damped wave equation*, which is central in Paper I. Consider the equation

$$\begin{aligned} \ddot{u} - \nabla \cdot (A\nabla\dot{u} + B\nabla u) &= f, \quad \text{in } D \times (0,T], \\ u &= 0, \quad \text{on } \partial D \times (0,T], \\ u(0) = u_0,\ \dot{u}(0) &= v_0, \quad \text{in } D. \end{aligned} \tag{2.2.10}$$

Here, D, A, f, u_0, v_0 are defined as for the standard wave equation, and $B = B(x)$ is another (possibly rapidly oscillating) coefficient independent of time. For the system (2.2.10), the coefficients A and B represents the damping and wave propagation of the solution, respectively. Note that the main difference between the standard wave equation and its strongly damped counterpart is the damping term $-\nabla \cdot A\nabla\dot{u}$. Consequently, the system (2.2.10) is not energy conserving. Instead, as the authors in [43] show, the solution satisfies a parabolic decay in similarity to that of (2.2.3).

By standard procedure, the backward Euler FEM for (2.2.10) becomes: find $u_h^n \in V_h$ for $n = 2, \ldots, N$, with initial values $u_h^0, u_h^1 \in V_h$, such that

$$(\bar{\partial}_t \bar{\partial}_t u_h^n, v) + a(\bar{\partial}_t u_h^n, v) + b(u_h^n, v) = (f^n, v), \tag{2.2.11}$$

holds for all $v \in V_h$, where $b(\cdot,\cdot) := (B\nabla\cdot, \nabla\cdot)$. Here, the temporal scheme corresponds to the backward Euler discretization, which can be seen by substituting $w_h^n = \bar{\partial}_t u_h^n$ and writing (2.2.11) as a system of first order equations. The error satisfies the estimate

$$\|u_h^n - u(t_n)\| \leq C(\tau + h^2/\min\{\varepsilon_A, \varepsilon_B\}).$$

Here, we have denoted by ε_A and ε_B the scales at which the damping A and the wave propagation B vary at, respectively. For the strongly damped wave

equation, we therefore require an approach which takes the oscillations of two different multiscale coefficients into account. This topic is dealt with in Paper I.

2.3 Stochastic PDEs

We conclude the chapter by demonstrating how the finite element method can be applied to stochastic partial differential equations (SPDEs). As model problem, we will consider a parabolic equation similar to (2.2.1), where the right-hand side data is driven by noise. Due to the randomness, the solution is generally characterized by its moments, rather than considering one distinct realization of the equation. First, we introduce the necessary preliminaries and notation for the stochastic setting. Then, we derive the fully discretized finite element method for the SPDE. Finally, we discuss Monte-Carlo simulations, applied to approximate the expectation of (some function of) the solution.

Notation and preliminaries

Prior to introducing the SPDE used as model problem, we require some basic preliminaries and notations. For further details on each concept, the reader is referred to the introductory chapter in [15]. Let Ω be a non-empty set, $\mathcal{F}$ a σ-algebra on Ω, $\mathbb{P} : \mathcal{F} \to [0,1]$ a probability measure, and $\{\mathcal{F}_t\}_{t\geq 0}$ a filtration. The quadruple $(\Omega, \mathcal{F}, \mathbb{P}, \{\mathcal{F}_t\}_{t\geq 0})$ is a called a *filtered probability space*.

Let $L(U;V)$ denote the space of linear bounded operators between two separable Hilbert spaces U and V, with the short-hand notation $L(V) := L(V;V)$ in the case $U = V$. Furthermore, denote by $L_N^+(U)$ the space of all non-negative, symmetric, nuclear operators on U. We assume W to be a Q-Wiener process with covariance operator $Q \in L_N^+(U)$. For details on covariance operators, we refer to [15, Chapter 2]. The covariance operator $Q \in L_N^+(U)$ satisfies the Hilbert–Schmidt theorem (see, e.g., [61, Theorem VI.16]), i.e., there is an orthonormal basis $\{e_i\}_{i=1}^\infty$ of U such that $Qe_i = \lambda_i e_i$, where $\lambda_i \to 0$ as $i \to \infty$. Consequently, the process W can be expressed (see [15, Proposition 4.3]) by its *Karhunen–Loève expansion*

$$W(t) = \sum_{i=1}^{\infty} \sqrt{\lambda_i}\beta_i(t)e_i, \tag{2.3.1}$$

where $\{\beta_i(t)\}_{i=1}^\infty$ are mutually independent, real-valued Brownian motions. We are now well-equipped to introduce the model problem.

Parabolic SPDE

We consider the parabolic SPDE

$$\begin{aligned} \mathrm{d}X + \Lambda X \,\mathrm{d}t &= G\,\mathrm{d}W, && \text{in } D \times (0,T], \\ X &= 0, && \text{on } \partial D \times (0,T], \\ X(0) &= X_0, && \text{in } D. \end{aligned} \tag{2.3.2}$$

where the solution X is a V-valued random process for some Hilbert space V. The diffusion operator $\Lambda := -\nabla \cdot A\nabla$ and the domain D are defined as in Section 2.1 and X_0 is the (possibly stochastic) initial value. The noise W is an U-valued Q-Wiener process defined on the filtered probability space $(\Omega, \mathcal{F}, \mathbb{P}, \{\mathcal{F}_t\}_{t\geq 0})$, and $G \in L(U;V)$ is an operator that maps the noise between the Hilbert spaces U and V.

Let E be the semigroup from Section 2.2. In line with Duhamel's principle for standard parabolic equations, the so-called *mild solution* to (2.3.2) is given by (see [15, Chapter 7])

$$X(t) = E(t)X_0 + \int_0^t E(t-s)G\,\mathrm{d}W(s), \tag{2.3.3}$$

where the stochastic integral is defined in the sense of Itô. In the finite element analysis of SPDEs (see, e.g., [67]), the error of the mild solution is in focus, instead of the weak solution. However, in [58], it is shown that under certain assumptions the weak and mild solution are equivalent. We quickly mention that in Paper IV, where the SPDE (2.3.2) is in focus, such assumptions hold.

For the spatial discretization of 2.3.2, let V_h be defined as in prior sections. The semi-discrete Galerkin method states: find $X_h(t) \in V_h$ such that

$$\mathrm{d}X_h + \Lambda_h X_h \,\mathrm{d}t = P_h G\,\mathrm{d}W, \tag{2.3.4}$$

with initial value $X_h^0 = P_h X_0$. Here, $\Lambda_h : V_h \to V_h$ is the discrete version of the operator Λ, defined by the relation

$$(\Lambda_h v, w) = a(v, w),$$

for all $v, w \in V_h$, and $P_h : L_2(D) \to V_h$ denotes the standard $L_2(D)$-projection onto V_h, i.e., for any function $v \in V$, $P_h v \in V_h$ satisfies

$$(P_h v, w) = (v, w), \tag{2.3.5}$$

for every $w \in V_h$.

Let the temporal domain $[0, T]$ be discretized as in Section 2.2, and denote $X_h^n := X_h(t_n)$. The backward Euler–Galerkin scheme of (2.3.4) is defined as

$$X_h^n - X_h^{n-1} + \tau \Lambda_h X_h^n = \int_{t_{n-1}}^{t_n} P_h G \, \mathrm{d}W(s). \tag{2.3.6}$$

Alternatively, define $E_{\tau,h} := (I + \tau \Lambda_h)^{-1}$, and (2.3.6) can be written as

$$X_h^n = E_{\tau,h} X_h^{n-1} + \int_{t_{n-1}}^{t_n} E_{\tau,h} P_h G \, \mathrm{d}W(s). \tag{2.3.7}$$

By further iterating this expression, we yield a discrete version of (2.3.3), i.e.,

$$X_h^n = E_{\tau,h}^n P_h X_0 + \sum_{j=1}^{n} \int_{t_{j-1}}^{t_j} E_{\tau,h}^{n-j+1} P_h G \, \mathrm{d}W(s).$$

If sufficient regularity is assumed on the initial value X_0 and the covariance operator Q, it holds that the finite element approximation X_h^n from (2.3.7) converges to the exact solution of (2.3.2) quadratically in space and linearly in time. In fact, by following the proof of [38, Theorem 3.14] and adjusting the calculations to our model problem, it is shown that the strong error satisfies the bound

$$\|X_h^n - X(t_n)\|_{L_2(\Omega; L_2(D))} \leq C(k^{\mu/2} + h^\mu/\varepsilon), \tag{2.3.8}$$

where $\mu \in [1, 2]$ depends on the regularity of X_0 and Q. The norm used for the strong error is defined as $\|\cdot\|_{L_2(\Omega; L_2(D))} := (\mathbb{E}[\|\cdot\|^2])^{1/2}$, where $\mathbb{E}$ denotes the standard expectation. In (2.3.8), we once again note that the finite element method requires a mesh size $h < \varepsilon$ to compute accurate approximations. In Paper IV, we introduce a method for which we derive an a priori result in similarity to (2.3.8), but independent of the scale ε.

Monte-Carlo simulation

In the previous section, we presented the error estimate in a strong sense, i.e., measured in mean-square. However, in many cases it is preferable to analyze the expectation of the solution, or more generally some function of the solution. For this purpose, let $g : L_2(D) \to \mathcal{B}$ be a Lipschitz continuous function with values in a separable Hilbert space $\mathcal{B}$. In this section, we focus on the error between $\mathbb{E}[g(X(t_n))]$ and its finite element approximation $\mathbb{E}[g(X_h^n)]$, referred

to as the *weak error*, given by

$$\|\mathbb{E}[g(X(t_n))] - \mathbb{E}[g(X_h^n)]\|_{\mathcal{B}}.$$

To measure this error, we are thus required to compute the expectation of the finite element approximation. However, since the solution X_h^n depends on the realization of the noise W, it is not obvious how the expectation behaves from one single simulation. Instead, an approximation of the expectation is computed by averaging over a large number of random samples, known as *Monte-Carlo simulation*. The expectation $\mathbb{E}[g(X_h^n)]$ is approximated by its Monte-Carlo estimator $E_M[g(X_h^n)]$ as

$$\mathbb{E}[g(X_h^n)] \approx E_M[g(X_h^n)] := \frac{1}{M}\sum_{m=1}^{M} g(X_h^{n,m}), \tag{2.3.9}$$

where $\{X_h^{n,m}\}_{m=1}^M$ are independent and identically distributed random variables with the same distribution as X_h^n.

The total weak error is now given by comparing $\mathbb{E}[g(X(t_n))]$ with the Monte-Carlo estimator $E_M[g(X_h^n)]$. We note that the error can be decomposed as

$$\begin{aligned}&\|\mathbb{E}[g(X(t_n))] - E_M[g(X_h^n)]\|_{L_2(\Omega;\mathcal{B})}\\ &\quad\le \|\mathbb{E}[g(X(t_n))] - \mathbb{E}[g(X_h^n)]\|_{\mathcal{B}} + \|\mathbb{E}[g(X_h^n)] - E_M[g(X_h^n)]\|_{L_2(\Omega;\mathcal{B})}.\end{aligned}$$

That is, one part that depends on the discretization error from the finite element scheme, and a second part, which is the statistical error from the Monte-Carlo estimation. For the discretization part, it follows that the weak error is bounded by the strong error, since

$$\begin{aligned}\|\mathbb{E}[g(X(t_n))] - \mathbb{E}[g(X_h^n)]\|_{\mathcal{B}}^2 &\le \mathbb{E}[\|g(X(t_n)) - g(X_h^n)\|_{\mathcal{B}}^2]\\ &\le L_g^2\mathbb{E}[\|X(t_n) - X_h^n\|^2]\\ &= L_g^2\|X(t_n) - X_h^n\|_{L_2(\Omega;L_2)}^2\\ &\le C(\tau + h^2/\varepsilon),\end{aligned} \tag{2.3.10}$$

where we first used Jensen's inequality, followed by the fact that g is Lipschitz continuous with constant L_g, and finally used the strong convergence bound from (2.3.8).

Remark 2.3.1. In (2.3.10) we used the strong convergence bound with $\mu = 2$, i.e., in the case of sufficient regularity on X_0 and Q, which corresponds to the optimal rate for piecewise linear polynomials. This choice was done to simplify the presentation of the weak error estimate. However, it is a well-established fact that the discretization error for SPDEs generally achieves twice

the order of weak convergence in comparison to the corresponding order of strong convergence (see, e.g., [9, 39, 37]). That is, the weak error generally achieves optimal order convergence in the case of lower regularity as well, i.e., when $\mu \in [1, 2)$.

The statistical error from the Monte-Carlo estimation depends on the variance in the solution X_h^n, as well as the number of samples M. Indeed, for the error, we note that

$$\begin{aligned}
&\|\mathbb{E}[g(X_h^n)] - E_M[g(X_h^n)]\|_{L_2(\Omega;\mathcal{B})}^2 \\
&\qquad = \mathbb{E}[\|\mathbb{E}[X_h^n] - E_M[X_h^n]\|_{\mathcal{B}}^2] \\
&\qquad = \mathbb{E}\left[\left\| \frac{1}{M} \sum_{m=1}^{M} (\mathbb{E}[g(X_h^n)] - g(X_h^{n,m})) \right\|_{\mathcal{B}}^2\right] \\
&\qquad = \frac{1}{M^2} \sum_{m=1}^{M} \mathbb{E}[\|\mathbb{E}[g(X_h^n)] - g(X_h^{n,m})]\|_{\mathcal{B}}^2] \\
&\qquad = \frac{1}{M} \mathbb{E}[\|\mathbb{E}[g(X_h^n)] - g(X_h^n)]\|_{\mathcal{B}}^2] \\
&\qquad = \frac{\mathbb{V}\mathrm{ar}\{g(X_h^n)\}}{M},
\end{aligned} \tag{2.3.11}$$

where, since $\mathbb{E}[\mathbb{E}[g(X_h^n)] - g(X_h^{n,m})] = 0$ and $\{X_h^{n,m}\}_{m=1}^M$ are all independent, the mixed term vanishes in the third equality.

In total, combining the discretization error bounded by (2.3.10) with the statistical error (2.3.11), the weak error satisfies the error estimate

$$\|\mathbb{E}[g(X(t_n))] - E_M[g(X_h^n)]\|_{L_2(\Omega;\mathcal{B})} \leq C\Big(\tau + h^2/\varepsilon + \frac{1}{\sqrt{M}}\Big). \tag{2.3.12}$$

At this point, we notice that in order to maintain the convergence rate, the number of Monte-Carlo simulations M needs to be proportional to the mesh size h as $M \sim h^{-4}$. However, recall that the scale ε adds the additional requirement that $h < \varepsilon$ for the convergence rate to be valid. In principle, this does not necessarily put an extra requirement on the number of Monte-Carlo simulations, but we remark that each simulation $X_h^{n,m}$ requires ε-dependent computations. That is, when multiscale features appear in SPDEs, the computational effort is even more negatively affected than the deterministic setting. In Paper IV, a multiscale method for SPDEs is used that circumvents the requirement $h < \varepsilon$, and consequently improves the computational efficiency significantly.

Multilevel Monte-Carlo

As previously stated, the Monte-Carlo estimator requires the number of samples to be to proportional to the mesh size as $M \sim h^{-4}$, where each sample is computed on the grid $\mathcal{T}_h$. An alternative approach is to consider the *multilevel Monte-Carlo estimator*, which reduces the computational complexity by allocating a large proportion of the samples to the coarser levels. In this way, the coarser grids can be used to cheaply compute the majority of the samples, which reduces the statistical error, while the finer levels are used to improve the deterministic accuracy.

The idea of the multilevel Monte-Carlo estimator for stochastic differential equations was first presented in [21], and is based on writing the expectation as a telescopic sum over the nested discretization levels. For this purpose, let h_j denote the mesh size corresponding to the discretization $\mathcal{T}_{h_j}$. Then, we write

$$\mathbb{E}[g(X^n_{h_J})] = \mathbb{E}[g(X^n_{h_0})] + \sum_{j=1}^{J} \mathbb{E}[g(X^n_{h_j}) - g(X^n_{h_{j-1}})].$$

In this way, we can estimate each term by a Monte-Carlo estimator with different sample size depending on the grid level. That is, the multilevel Monte-Carlo estimator is given by

$$\begin{aligned} E^J[g(X^n_{h_J})] &:= E_{M_0}[g(X^n_{h_0})] + \sum_{j=1}^{J} E_{M_j}[g(X^n_{h_j}) - g(X^n_{h_{j-1}})] \\ &= \frac{1}{M_0}\sum_{m=1}^{M_0} g(X^{n,m}_{h_0}) + \sum_{j=1}^{J} \frac{1}{M_j}\sum_{m=1}^{M_j} g(X^{n,m}_{h_j}) - g(X^{n,m}_{h_{j-1}}). \end{aligned} \tag{2.3.13}$$

where M_j denotes the number of samples used on the discretization level $\mathcal{T}_{h_j}$ and $E_{M_j}[\cdot]$ is defined as in (2.3.9).

The advantage of the multilevel approach is that we can choose $\{M_j\}_{j=0}^J$ such that the majority of the samples are allocated to the coarser levels, while the weak convergence rate from the Monte-Carlo estimator is maintained. Indeed, if we repeat the calculations in [8, Corollary 3.8], it is shown that the multilevel estimator satisfies

$$\|\mathbb{E}[g(X(t_n))] - E^J[g(X^n_{h_J})]\|_{L_2(\Omega;\mathcal{B})} \leq C\Big(\tau + \frac{h_J^2}{\varepsilon} + \frac{1}{\sqrt{M_0}} + \frac{1}{\varepsilon}\sum_{j=1}^{J} \frac{h_j^2}{\sqrt{M_j}}\Big).$$

We want to choose the number of samples $\{M_j\}_{j=0}^J$ such that the convergence rate from (2.3.12) is retrieved. For instance, one choice that works is to set $M_0 = \gamma h_J^{-4}$, where γ is some proportionality constant, and $M_j = M_0 h_j^4 \cdot 2^{2\delta j}$ for some $\delta > 0$. Then, the final sum satisfies

$$\sum_{j=1}^{J} \frac{h_j^2}{\sqrt{M_j}} = \sum_{j=1}^{J} \frac{1}{\sqrt{M_0 \cdot 2^{2\delta j}}} = \frac{1}{\sqrt{M_0}} \sum_{j=1}^{J} 2^{-\delta j} \leq \gamma^{-1/2} h_J^2 \frac{1}{2^\delta - 1},$$

where the final inequality bounds the geometric sum by its limit as $J \to \infty$. We remark that a large δ implies a better constant in the error estimate, but yields a slower decay in the number of samples $\{M_j\}_{j=0}^J$, and vice-versa for a small δ. In this way, the parameter δ controls the trade-off between the constant in the error estimate and the computational complexity of the method.

While the multilevel Monte-Carlo estimator reduces the overall complexity, it still holds that the high variations in the diffusion brings the scale ε into the estimate, such that the requirement $h_J < \varepsilon$ must hold for the convergence rate to be valid. In Paper IV, the multilevel estimator is combined with a multiscale approach that removes this requirement, which results in an efficient method that instantly achieves the sought convergence rate.

We have so far considered several different equations of both stationary, evolution and stochastic type, and discussed the main results from their corresponding well-established finite element methods. As repeatedly pointed out, in neither case, the spatial convergence satisfies optimal rate unless the mesh size is sufficiently refined. In subsequent chapter, we introduce the multiscale method known as the localized orthogonal decomposition method, developed to circumvent the difficulty of varying data.

3 Localized orthogonal decomposition (LOD)

For the purpose of solving PDEs with rapidly varying data, several multiscale methods have been developed. In this thesis the focus lies on the localized orthogonal decomposition (LOD) method, first introduced in [51]. Widely speaking, the LOD method is based on a decomposition of the solution space into a coarse and a fine part. The fine part is assumed to be refined enough to be able to resolve the variations in the data, while the coarse part is used for the main (cheap) computations. In short, the goal is to enrich the coarse-scale space by problem-dependent data computed on the fine scale. This yields a coarse-scale modification of the original problem that efficiently approximate solutions with accuracy independent of the data variations.

This chapter is divided into two parts. Firstly, we derive and illustrate the performance of the LOD method in the elliptic setting, and compare it to the finite element method presented in Section 2.1. Moreover, we demonstrate how the LOD technique is applied to general matrix systems. Secondly, we extend the LOD framework to the time-dependent setting, and discuss its computational benefits.

3.1 LOD in the elliptic setting

We begin by introducing the method corresponding to the elliptic case, using the equation defined in (2.1.1) as model problem. At first, we derive the method in its ideal case. However, there are computational difficulties arising in this method due to the resulting matrix systems not being sparse, but dense. For this purpose, a localized version that is computationally feasible is presented. We continue by revisiting the numerical example from Section 2.1. Finally, we

consider general matrix systems of the form (2.1.4) and show how the LOD method can be applied to efficiently approximate solutions to such equations.

3.1.1 Ideal method

At first, assume the mesh size h to be fixed and sufficiently small, i.e., $h < \varepsilon$, so that the FE-space V_h can approximate the solution accurately. We define the space V_H similarly to V_h but with a larger mesh size $H > h$. Moreover, let $\mathcal{N}$ denote the set of interior nodes of $\mathcal{T}_H$, and $\{\lambda_x\}_{x\in\mathcal{N}}$ be the set of standard piecewise linear basis functions such that

$$V_H = \operatorname{span}(\{\lambda_x\}_{x\in\mathcal{N}}).$$

Recall that computing a solution in V_H is cheap, but inaccurate as described in Section 2.1. The goal of LOD is to incorporate the finescale behavior of the diffusion into V_H to define a new so-called *multiscale space* V_{ms}, which has the property that $\dim(V_{\mathrm{ms}}) = \dim(V_H)$, so that the computations are cheap, but with an error bound independent of ε.

For the construction of the multiscale space we require an interpolant $I_H : V_h \to V_H$ with the projection property $I_H \circ I_H = I_H$ that for all $T \in \mathcal{T}_H$ and any function $v \in V_h$ satisfies

$$H_T^{-1}\|v - I_H v\|_{L_2(T)} + \|\nabla I_H v\|_{L_2(T)} \leq C_I \|\nabla v\|_{L_2(N(T))}, \tag{3.1.1}$$

where $N(T) := \{T' \in \mathcal{T}_H : \overline{T'} \cap \overline{T} \neq \emptyset\}$ and $H_T := \operatorname{diam}(T)$. Furthermore, for a shape-regular and quasi-uniform partition, the estimate (3.1.1) can be summed into the global estimate

$$H^{-1}\|v - I_H v\| + \|\nabla I_H v\| \leq C_\gamma \|\nabla v\|, \tag{3.1.2}$$

where C_γ depends on the interpolation constant C_I and the shape regularity parameter defined as

$$\gamma := \max_{T\in\mathcal{T}_H} \gamma_T, \text{ where } \gamma_T := \frac{\operatorname{diam}(B_T)}{H_T}.$$

Here B_T denotes the largest ball inside of T. There are several choices of interpolants that can be used for the construction. A commonly used example, used for the numerical examples in Papers I, II and IV, is $I_H = E_H \circ \Pi_H$, where Π_H is the piecewise L_2-projection onto $P_1(\mathcal{T}_H)$, the space of affine functions on each triangle $T \in \mathcal{T}_H$, and $E_H : P_1(\mathcal{T}_H) \to V_H$ is an averaging operator that, to each free node $x \in \mathcal{N}$, assigns the arithmetic mean of corresponding function

values on intersecting elements, i.e.,

$$(E_H(v))(x) = \frac{1}{\text{card}\{T \in \mathcal{T}_H : x \in \overline{T}\}} \sum_{T \in \mathcal{T}_H \,:\, x \in \overline{T}} v\big|_T(x).$$

For a more detailed discussion regarding possible choices of the interpolant, see, e.g., [19] or [59].

For any function $v \in H_0^1$, $I_H v$ describes the coarse part of the solution in the space V_H. The remainder part $(1 - I_H)v$ contains fine-scale features of v that are not captured by the coarse space. These fine-scale functions configure the so-called fine-scale space, defined by the kernel of the interpolant, i.e.,

$$V_{\mathrm{f}} := \ker(I_H) = \{v \in V_h : I_H v = 0\}.$$

That is, V_{f} consists of the fine-scale features of the solution which the finite elment space is unable to capture. Consequently, this leads to the solution space being decomposed as

$$V_h = V_H \oplus V_{\mathrm{f}},$$

so that every function $v \in V_h$ can be uniquely written as $v = v_H + v_{\mathrm{f}}$ where $v_H \in V_H$ and $v_{\mathrm{f}} \in V_{\mathrm{f}}$.

The LOD method is characterized by correcting coarse functions by an appropriate projection into V_{f}. Thus, let $\mathcal{Q}_{\mathrm{f}} : V_h \to V_{\mathrm{f}}$ be the Ritz-projection onto V_{f}, i.e., $\mathcal{Q}_{\mathrm{f}} v \in V_{\mathrm{f}}$ satisfies the relation

$$a(\mathcal{Q}_{\mathrm{f}} v, w) = a(v, w),$$

for all $w \in V_{\mathrm{f}}$. Using this Ritz-projection we create our multiscale space as

$$V_{\mathrm{ms}} := V_H - \mathcal{Q}_{\mathrm{f}} V_H.$$

Note that for all $v_{\mathrm{ms}} \in V_{\mathrm{ms}}$ and $v_{\mathrm{f}} \in V_{\mathrm{f}}$ it holds that

$$a(v_{\mathrm{ms}}, v_{\mathrm{f}}) = a(v_H - \mathcal{Q}_{\mathrm{f}} v_H, v_{\mathrm{f}}) = a(v_H, v_{\mathrm{f}}) - a(\mathcal{Q}_{\mathrm{f}} v_H, v_{\mathrm{f}}) = 0.$$

Hence, the Ritz-projection $\mathcal{Q}_{\mathrm{f}}$ yields an orthogonal splitting with respect to the bilinear form $a(\cdot, \cdot)$ as

$$V_h = V_{\mathrm{ms}} \oplus V_{\mathrm{f}}.$$

Since V_{ms} is the orthogonal complement to V_{f} it holds that $\dim(V_{\mathrm{ms}}) = \dim(V_H)$, but unlike V_H it moreover contains fine-scale features of the dif-

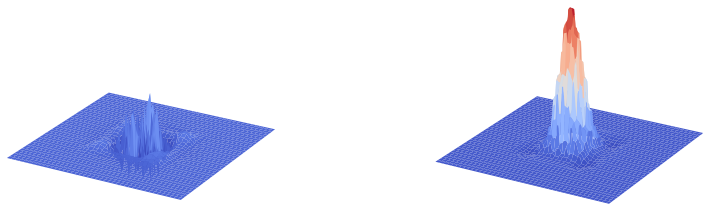

(a) ϕ_x. **(b)** $\lambda_x - \phi_x$.

Figure 3.1: The basis correction ϕ_x (left) and corresponding modified basis function $\lambda_x - \phi_x$ (right) for a coarse node $x \in \mathcal{N}$ positioned at $(0.375, 0.500)$ in the unit square.

fusion due to the Ritz-projection.

For the construction of the multiscale space, we want to compute the projection for a fixed set of functions. Hence, we use the Ritz-projection to define the basis corrector $\phi_x := \mathcal{Q}_{\mathrm{f}}\lambda_x \in V_{\mathrm{f}}$ for each coarse node $x \in \mathcal{N}$ as the solution to the (global) corrector problem

$$a(\phi_x, w) = a(\lambda_x, w), \tag{3.1.3}$$

for all $w \in V_{\mathrm{f}}$. The basis for V_{ms} is then given by $\{\lambda_x - \phi_x\}_{x\in\mathcal{N}}$, which can be viewed as a modified basis that incorporates fine-scale features of the diffusion coefficient. An example of a computed basis corrector ϕ_x and its corresponding modified basis function $\lambda_x - \phi_x$ is illustrated in Figure 3.1.

Given the multiscale space, the ideal LOD method reads: find $u_{\mathrm{ms}} \in V_{\mathrm{ms}}$ such that

$$a(u_{\mathrm{ms}}, v) = (f, v), \tag{3.1.4}$$

holds for all $v \in V_{\mathrm{ms}}$. In [51], the following theorem on an a priori error bound is derived for the method.

Theorem 3.1.1. *Let u_h be the solution to* (2.1.3) *and u_{ms} the solution to* (3.1.4)*. Then the error is bounded by*

$$\|u_{\mathrm{ms}} - u_h\|_{H^1} \leq CH\|f\|,$$

where C is independent of the variations in A, but depends on the upper and lower bound of A.

Proof. Let $e := u_{\mathrm{ms}} - u_h$ and note that $e \in V_{\mathrm{f}}$ due to the orthogonal splitting. Hence it holds that $I_H e = 0$. Moreover, recall the Galerkin orthogonality $a(e, v_{\mathrm{ms}}) = 0$ for $v_{\mathrm{ms}} \in V_{\mathrm{ms}}$. We get

$$a(e,e) = -a(u_h,e) = -(f,e) \leq \|f\|\|e\| = \|f\|\|e - I_H e\| \leq CH\|f\|\|e\|_{H^1},$$

where the final inequality follows from the interpolation estimate (3.1.2). The desired estimate now follows from the equivalence of norms between the H^1-norm and the norm induced by $a(\cdot,\cdot)$. □

The theorem states that the ideal LOD method achieves convergence of optimal order, but unlike the standard FEM, with a constant independent of the variations in A. Although the method seems promising, it is in its current state based on the global projection (3.1.3) onto the fine-scale space V_{f}. That is, it is as expensive to solve for one basis corrector as solving the finite element problem (2.1.3) on the fine scale. Moreover, by definition, each basis corrector ϕ_x has a global support which consequently makes the linear system corresponding to (3.1.4) dense. To circumvent these issues, we wish to localize the computations onto coarse patches in order to obtain a sparse matrix system. This act of localization is justified by the fact that each basis correction ϕ_x decays exponentially fast away from its corresponding node $x \in \mathcal{N}$, as proven in [51].

3.1.2 Localized method

To localize the corrector problem, we begin by defining the patches to which the support of each basis function is to be restricted. For $\omega \subset D$, let $N(\omega) := \{T \in \mathcal{T}_H : \overline{T} \cap \overline{\omega} \neq \emptyset\}$, and define a patch $N^k(\omega)$ of size k as

$$\begin{aligned} N^1(\omega) &:= N(\omega), \\ N^k(\omega) &:= N(N^{k-1}(\omega)), \quad \text{for } k \geq 2. \end{aligned}$$

Given a coarse grid patch, we may restrict the finescale space V_{f} to it by defining

$$V_{\mathrm{f},k}^{\omega} := \{v \in V_{\mathrm{f}} : \mathrm{supp}(v) \subseteq N^k(\omega)\}.$$

In particular, we will commonly use $\omega = T \in \mathcal{T}_H$ and $\omega = x \in \mathcal{N}$ as subdomains. An example of how the patches spread across the grid with increasing k is illustrated in Figure 3.2.

We aim to localize the computation and support of the basis corrector ϕ_x by utilizing the newly defined coarse patches. For this purpose, define the element

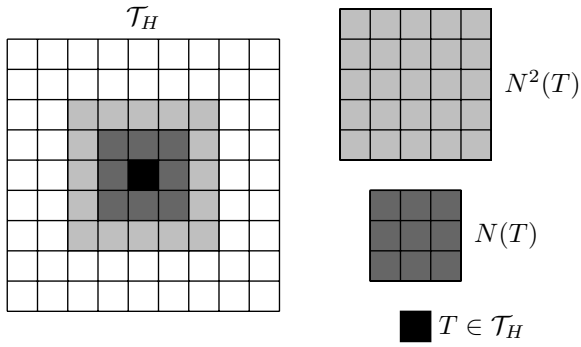

Figure 3.2: Illustration of patches based on an element $T \in \mathcal{T}_H$.

restricted Ritz-projection $\mathcal{Q}_{\mathrm{f}}^T$ such that $\mathcal{Q}_{\mathrm{f}}^T v \in V_{\mathrm{f}}$ is the solution to the system

$$a(\mathcal{Q}_{\mathrm{f}}^T v, w) = \int_T A\nabla v \cdot \nabla w \,\mathrm{d}x,$$

for all $w \in V_{\mathrm{f}}$. Note here that if we sum over all elements $T \in \mathcal{T}_H$ we get

$$a\Big(\sum_T \mathcal{Q}_{\mathrm{f}}^T v, w\Big) = \sum_T a(\mathcal{Q}_{\mathrm{f}}^T v, w) = \sum_T \int_T A\nabla v \cdot \nabla w \,\mathrm{d}x = a(v, w),$$

for any function $w \in V_{\mathrm{f}}$. That is, the global Ritz-projection is constructed by the summation

$$\mathcal{Q}_{\mathrm{f}} v = \sum_{T \in \mathcal{T}_H} \mathcal{Q}_{\mathrm{f}}^T v.$$

For $k \in \mathbb{N}$, we may restrict the projection to a patch by letting $\mathcal{Q}_{\mathrm{f},k}^T : V_H \to V_{\mathrm{f},k}^T$ be such that $\mathcal{Q}_{\mathrm{f},k}^T v \in V_{\mathrm{f},k}^T$ solves

$$a(\mathcal{Q}_{\mathrm{f},k}^T v, w) = \int_T A\nabla v \cdot \nabla w \,\mathrm{d}x,$$

for all $w \in V_{\mathrm{f},k}^T$. By summation this yields the corresponding global version as

$$\mathcal{Q}_{\mathrm{f},k} v = \sum_{T \in \mathcal{T}_H} \mathcal{Q}_{\mathrm{f},k}^T v.$$

Finally, we may construct a localized multiscale space as $V_{\mathrm{ms},k} := V_H - \mathcal{Q}_{\mathrm{f},k} V_H$, spanned by $\{\lambda_x - \mathcal{Q}_{\mathrm{f},k}\lambda_x\}_{x \in \mathcal{N}}$.

We replace the multiscale space V_{ms} by its localized version $V_{\mathrm{ms},k}$ and obtain

the localized LOD method that reads: find $u_{\mathrm{ms},k} \in V_{\mathrm{ms},k}$ such that

$$a(u_{\mathrm{ms},k}, v) = (f, v), \tag{3.1.5}$$

holds for all $v \in V_{\mathrm{ms},k}$. For a given element $T \in \mathcal{T}_H$, the dimension of $V_{\mathrm{f},k}^T$ is significantly smaller than that of V_{f}. Hence, the problem of finding $\mathcal{Q}_{\mathrm{f},k}\lambda_x$ is computationally cheaper than finding $\mathcal{Q}_{\mathrm{f}}\lambda_x$. Moreover, due to the restricted support of the basis correctors, the resulting linear system is also sparse (where the sparsity is determined by the size of the corresponding grid patches). Another computational benefit is that the corrector problems are all independent and can be solved in parallel.

In [26], the following theorem is proved for the error bound.

Theorem 3.1.2. *Let u_h be the solution to* (2.1.3) *and $u_{\mathrm{ms},k}$ the solution to* (3.1.5)*. Then there exists $\xi \in (0,1)$ such that*

$$\|u_{\mathrm{ms},k} - u_h\|_{H^1} \leq C(H + k^{d/2}\xi^k)\|f\|,$$

where C is independent of the variations in A, but depends on the upper and lower bound of A.

The convergence is thus dependent on the choice of k. To achieve linear convergence for the method, k should be chosen proportional to $\log(1/H)$.

3.1.3 Numerical example

To demonstrate the performance of the LOD method we revisit the example from Section 2.1. Once again the domain is set to the unit square, and the same coefficient as defined in (2.1.5) is used, where the scale at which the values vary is set to $\varepsilon = 2^{-6}$. The fine mesh is once again set to $h = 2^{-8}$ so that it resolves the fine variations of the coefficient. We compute the localized solution $u_{\mathrm{ms},k}$, where $k = \log_2(1/H)$, for $H = 2^{-2}, \ldots, 2^{-6}$ and plot the energy error $|||u_{\mathrm{ms},k} - u_{\mathrm{ref}}|||$ where the reference solution u_{ref} is obtained using the finite element method on the fine mesh. For comparison, we also plot the error of the finite element solution based on the same mesh sizes. The error plot can be seen in Figure 3.3 and shows how the FEM-error remains on a constant level throughout all mesh sizes, while the LOD-error instantly decays according to the established theory.

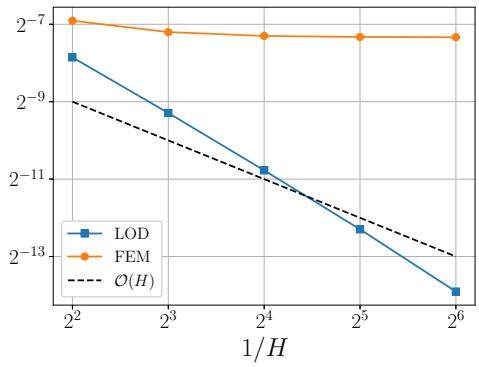

Figure 3.3: The energy error $|||u_{\mathrm{ms},k} - u_{\mathrm{ref}}|||$ (blue) for different coarse mesh sizes H. For comparison, the FEM-error $|||u_H - u_{\mathrm{ref}}|||$ (orange) is also plotted. The dashed line is an $\mathcal{O}(H)$-reference line.

3.1.4 Discrete setting

We conclude the section on stationary problems by illustrating how the LOD method can be extended to general discrete systems characterized by a symmetric, positive definite matrix K. The matrix K can for instance represent, but is not limited to, a finite difference stencil or the graph Laplacian. This particular extension of the LOD method was first introduced in [35], and was further justified theoretically in [17]. As model problem, we consider a weak formulation of the system (2.1.4). That is, we seek $u \in V$ such that for all $v \in V$ it holds

$$(Ku, v) = (f, v). \tag{3.1.6}$$

Here, V is a discrete solution space, e.g., some subset of $\mathbb{R}^n$ with some Dirichlet nodes fixed where the solution is equal to zero, f the right-hand side data, and $(\cdot, \cdot)$ the Euclidean scalar product.

Whenever the matrix K contains high variations in its data, the system becomes ill-conditioned and only direct solvers are applicable. As this becomes highly inefficient as the system grows larger, we apply the LOD method to efficiently find an approximate solution to (3.1.6). In similarity to the continuous LOD setting, we introduce an interpolation matrix $I : V \to V$. For now, we mention that the matrix could, for instance, represent a discrete version of the Clément-type interpolant. In Section 4.3, the construction and main properties of I are discussed in more detail.

With the interpolant I, we are able to capture the coarse behavior of any function in V. The remaining part is recovered in the fine-scale space $W := \ker(I) \subset V$. In this way, we define the multiscale space V_{ms} as the functions in V that are orthogonal to W with respect to the matrix K, i.e.,

$$V_{\mathrm{ms}} := \{v \in V : (Kv, w) = 0, \, \forall w \in W\}.$$

Similarly to the continuous LOD setting, the computation of V_{ms} is based on a corrector-type problem as in that of (3.1.3), but with respect to the scalar product $(K\cdot, \cdot)$. In [17], the authors show that under the right assumptions, the correctors can be computed on local patches without losing essential information. Thus, by applying a localization procedure similar to that of the standard LOD method, one yields the localized space $V_{\mathrm{ms},k}$. We arrive at the method to find $u_{\mathrm{ms},k} \in V_{\mathrm{ms},k}$ such that

$$(Ku_{\mathrm{ms},k}, v) = (f, v), \tag{3.1.7}$$

holds for all $v \in V_{\mathrm{ms},k}$. With this method, we are able to efficiently compute accurate approximations to (3.1.6) independent of potential data variations in K. Indeed, in [17, Theorem 4.8], an a priori error estimate analogous to that of Theorem 3.1.1 is derived for the method (3.1.7). In Section 4.3, we discuss the discrete LOD method in detail and demonstrate how it is applicable to time-dependent settings. This extension to time-dependent matrix equations, with particular focus on the application to fiber networks, is the central topic of Paper III.

3.2 LOD for time-dependent problems

In this section, we discuss the LOD method in the time-dependent setting. In particular, we seek to highlight the additional computational efficiency that is gained in contrast to the stationary cases. For this purpose, we revisit the parabolic equation (2.2.1) as model problem. Similarly to the elliptic case, the LOD method follows by replacing the finite element space V_h by the localized multiscale space $V_{\mathrm{ms},k}$. This yields the LOD method: find $u^n_{\mathrm{ms},k} \in V_{\mathrm{ms},k}$ for $n \geq 1$, with initial value $u^0_{\mathrm{ms},k} \in V_{\mathrm{ms},k}$, such that

$$(\bar{\partial}_t u^n_{\mathrm{ms},k}, v) + a(u^n_{\mathrm{ms},k}) = (f^n, v), \tag{3.2.1}$$

holds for all $v \in V_{\mathrm{ms},k}$. The LOD method for parabolic equations (and its semilinear counterpart) have been studied in detail in [50]. In particular, the authors derive the following bound for the error between the LOD approximation and

the standard finite element approximation computed on the fine scale.

Theorem 3.2.1. *Let $u^n_{\mathrm{ms},k} \in V_{\mathrm{ms},k}$ be the solution to* (3.2.1)*, and $u^n_h \in V_h$ the solution to* (2.2.5)*. Then, there exists $\xi \in (0,1)$ such that the error satisfies*

$$\|u^n_{\mathrm{ms},k} - u^n_h\| \leq C(H + k^{d/2}\xi^k)^2,$$

where C is independent of the variations in the diffusion A, but depends on, e.g., the contrast in A.

Note that Theorem 3.2.1 implicitly yields optimal convergence between the LOD approximation and the analytical solution, since

$$\|u^n_{\mathrm{ms},k} - u^n_h\| \leq \|u^n_{\mathrm{ms},k} - u(t_n)\| + \|u(t_n) - u^n_h\|,$$

where the bound on the second term follows by standard finite element theory.

We have illustrated how the multiscale space $V_{\mathrm{ms},k}$ is used to achieve optimal order convergence independently of the variations in the diffusion, for both elliptic and parabolic equations. From a computational point of view, we remark that the computation of $V_{\mathrm{ms},k}$ is not cheap, as it involves solving several corrector problems on the fine scale. However, as previously emphasized, the corrector problems are all independent, and can therefore be solved in parallel, reducing the computational effort. Moreover, the LOD method gains an additional advantage in the time-dependent setting, since it is sufficient to compute $V_{\mathrm{ms},k}$ once, and then re-use it in each time step. This property is also taken advantage of when applying LOD to the linear wave equation, which has been thoroughly studied in [2]. In Paper IV, where a stochastic PDE is considered, the re-usability is of even further interest, as the Monte-Carlo approximation requires us to solve the equation an extensive number of times, as pointed out in Section 2.3.

So far we have seen that, even for time-dependent equations, it suffices to replace the finite element space by the multiscale space to define an efficient method that yields convergence of optimal order. However, this is not always the case. For instance, in the case of time-dependent diffusion $A = A(t,x)$, the multiscale space changes over time as well, and needs to be reconstructed for each time step. Such a case, when the changes over time moreover contain rapid oscillations, is considered in Paper II. We also note the space $V_{\mathrm{ms},k}$ only needs to take one coefficient into account in its construction. In the strongly damped wave equation, defined in (2.2.10), there are two multiscale coefficients that vary independently from each other. The corresponding LOD method must therefore take the behavior of both coefficients into account. An extensive study of this case is done in Paper I.

4 LOD for evolution problems

The LOD method as presented so far is well-established for various types of equations. In the previous chapter, its effectiveness for basic stationary and time-dependent equations was demonstrated. This chapter further extends the LOD approach and applies it to more complicated evolution problems.

As a first example, we consider the strongly damped wave equation that consists of two different multiscale coefficients. Here, the way the solution depends on the different coefficients is strongly affected by what phase of the time interval we consider. Hence the multiscale space must be constructed so that it is automatically adjusted for this effect over time. In Paper I, a GFEM that achieves this is derived and analyzed. The second case we consider is a parabolic equation, where we let the diffusion be time-dependent with rapid variations in both time and space. The LOD method for parabolic equations was rigorously analyzed in [50], but is only applicable for high oscillations in the spatial sense. An extension of the LOD method to the space- and time-dependent case is developed in Paper II. In [35, 17], the LOD framework was applied to general matrix systems in the stationary setting. Continuing their work, Paper III extends the technique to the time-dependent case by considering a discretized version of the linear wave equation, characterized by a symmetric, positive-definite matrix K. Finally, Paper IV presents a priori analysis for the LOD technique for stochastic partial differential equations, for which the reduced computational complexity is even more advantageous due to the Monte-Carlo sampling.

4.1 Strongly damped wave equation

Consider the strongly damped wave equation

$$\begin{aligned} \ddot{u} - \nabla \cdot (A\nabla\dot{u} + B\nabla u) &= f, && \text{in } D \times (0,T], \\ u &= 0, && \text{on } \partial D \times (0,T], \\ u(0) &= u_0, && \text{in } D, \\ \dot{u}(0) &= v_0, && \text{in } D, \end{aligned} \tag{4.1.1}$$

where $T > 0$ and D is a polygonal (or polyhedral) domain in $\mathbb{R}^d,\ d = 2, 3$. Here $A = A(x)$ represents the damping coefficient, $B = B(x)$ represents the wave propagation speed, $f = f(t, x)$ denotes the source function of the system, and the solution u is a displacement function. This equation is common in the modeling of viscoelastic materials, where the strong damping $-\nabla \cdot A\nabla\dot{u}$ appears when representing the stress as the sum of an elastic part and a viscous part [12, 22]. Viscoelastic materials have several applications in engineering, including noise dampening, vibration isolation, and shock absorption (see [34] for more applications). In multiscale applications, both A and B are rapidly varying. It is noteworthy that the solution is highly dependent on the damping A in the transient phase due to the time derivative, and that in the steady state phase it solely depends on the wave propagation speed B.

Recent years have seen extensive analysis on the strongly damped wave equation. For instance, well-posedness of the equation is discussed in [13, 33, 36], asymptotic behavior in [14, 5, 55], solution blowup in [20, 4], and decay estimates in [32]. In particular, the FEM for the strongly damped wave equation has been analyzed in [44] using the Ritz–Volterra projection, and [43] uses the classical Ritz-projection in the homogeneous case with Rayleigh damping.

Standard finite elements

We begin by considering the finite element method that corresponds to the system (4.1.1). For the spatial discretization of the problem, let V_h be defined as in Section 2.1. The semi-discrete FEM becomes: find $u_h(t) \in V_h$ such that for all $v \in V_h$, it holds

$$(\ddot{u}_h, v) + a(\dot{u}_h, v) + b(u_h, v) = (f, v), \quad t > 0,$$

with initial values $u_h(0) = u_{h,0}$ and $\dot{u}_h = v_{h,0}$, where $u_{h,0}, v_{h,0} \in V_h$ are appropriate approximations of u_0 and v_0 respectively. Here, the bilinear forms

are defined as $a(\cdot,\cdot) := (A\nabla\cdot, \nabla\cdot)$ and $b(\cdot,\cdot) := (B\nabla\cdot, \nabla\cdot)$.

For the temporal discretization, let $0 =: t_0 < t_1 < ... < t_N := T$ be a partition with uniform time step $\tau := t_n - t_{n-1}$. By applying a backward Euler scheme, the fully discrete system reads: find $u_h^n \in V_h$ for $n \geq 2$ such that

$$(\bar{\partial}_t^2 u_h^n, v) + a(\bar{\partial}_t u_h^n, v) + b(u_h^n, v) = (f^n, v), \tag{4.1.2}$$

for all $v \in V_h$. The first initial value is given by $u_h^0 \in V_h$. The second initial value u_h^1 should be an approximation of $u(t_1)$ and can, e.g., be chosen as $u_h^1 = u_h^0 + \tau v_h^0$. For results on regularity and error estimates, we refer to [43]. However, although convergence of optimal order is proven here, the involved constants are dependent on the variations in the coefficients A and B, and hence not applicable in the multiscale case.

Ideal GFEM

For the development of our GFEM for the strongly damped wave equation, we begin by defining the coarse FE-space V_H and the fine-scale space $V_{\mathrm{f}} := \ker(I_H)$ in complete analogy to Section 3.1. For the standard LOD method (as used in the elliptic case [51, 28, 26], parabolic case [50, 49], and for the wave equation [2, 47]), the definition of the Ritz-projection is based on solely the diffusion coefficient. However, since we have two different multiscale coefficients to incorporate in this case, we define the Ritz-projection $R_{\mathrm{f}} : V_H \to V_{\mathrm{f}}$ such that $R_{\mathrm{f}} v \in V_{\mathrm{f}}$ satisfies

$$a(R_{\mathrm{f}} v, w) + \tau b(R_{\mathrm{f}} v, w) = a(v, w) + \tau b(v, w), \tag{4.1.3}$$

for all $w \in V_{\mathrm{f}}$. Here, the operator R_{f} takes the role of $\mathcal{Q}_{\mathrm{f}}$ from Section 3.1, but considers both coefficients A and B in the projection. The particular choice of scalar product, $a(\cdot,\cdot) + \tau b(\cdot,\cdot)$, comes from the backward Euler scheme. Using this projection, we may define the multiscale space $V_{\mathrm{ms}} := V_H - R_{\mathrm{f}} V_H$ such that

$$V_h = V_{\mathrm{ms}} \oplus V_{\mathrm{f}}, \quad \text{and} \quad a(v_{\mathrm{ms}}, v_{\mathrm{f}}) + \tau b(v_{\mathrm{ms}}, v_{\mathrm{f}}) = 0.$$

The basis functions for this multiscale space is, similarly to the standard LOD method, defined by applying the Ritz-projection to the finite element basis function. That is, $R_{\mathrm{f}}\lambda_x \in V_{\mathrm{f}}$ solves the global corrector problem

$$a(R_{\mathrm{f}}\lambda_x, w) + \tau b(R_{\mathrm{f}}\lambda_x, w) = a(\lambda_x, w) + \tau b(\lambda_x, w), \tag{4.1.4}$$

for all $w \in V_{\mathrm{f}}$. The basis for V_{ms} can now be constructed as $\{\lambda_x - R_{\mathrm{f}}\lambda_x\}_{x\in\mathcal{N}}$, where $R_{\mathrm{f}}\lambda_x$ contains fine-scale information on both of the multiscale coeffi-

cients.

We may now formulate our ideal method. Since the solution space can be decomposed as $V_h = V_{\mathrm{ms}} \oplus V_{\mathrm{f}}$, the idea is to solve a coarse-scale problem in V_{ms}, and then add additional fine-scale corrections to account for the time-dependency of the problem. Note that this differs from the standard LOD method, where solving a system in V_{ms} suffices. By incorporating the correction, the solution can adapt so that its dependency on the coefficients A and B changes over time. In Remark 4.1.1, it is demonstrated how the added correction changes the solution from being orthogonal with respect to A in the transient phase to its B-orthogonality in the steady state phase.

The method reads: find $u_{\mathrm{lod}}^n = v^n + w^n$ for $n \geq 2$, where $v^n \in V_{\mathrm{ms}}$ satisfies

$$\tau(\bar{\partial}_t^2 v^n, z) + a(v^n, z) + \tau b(v^n, z) = \tau(f^n, z) + a(u_{\mathrm{lod}}^{n-1}, z), \tag{4.1.5}$$

for all $z \in V_{\mathrm{ms}}$, and $w^n \in V_{\mathrm{f}}$ satisfies

$$a(w^n, z) + \tau b(w^n, z) = a(u_{\mathrm{lod}}^{n-1}, z), \tag{4.1.6}$$

for all $z \in V_{\mathrm{f}}$, with initial data $u_{\mathrm{lod}}^0 = u_h^0 \in V_{\mathrm{ms}}$ and $u_{\mathrm{lod}}^1 = u_h^1 \in V_{\mathrm{ms}}$. The initial data is chosen in V_{ms} to simplify the implementation of the fine-scale correctors. This choice does not affect the performance of the proposed method, as shown in Paper I.

Remark 4.1.1. As earlier mentioned, the behavior of the damping A typically dominates the solution to (4.1.1) in the transient phase, while the solution depends more heavily on B if it reaches a steady state. Indeed, we note that the multiscale space V_{ms} is based on the correction (4.1.3) with small time step τ. That is, the correction in V_{ms} is initially dominated by A. However, in a steady state, it holds that $u_{\mathrm{lod}}^n \approx u_{\mathrm{lod}}^{n-1}$. Therefore, we note that by (4.1.6) it holds that for any $z \in V_{\mathrm{f}}$

$$\begin{aligned} a(w^n, z) + \tau b(w^n, z) &= a(u_{\mathrm{lod}}^{n-1}, z) \approx a(u_{\mathrm{lod}}^n, z) \\ &= a(v^n, z) + a(w^n, z) \\ &= -\tau b(v^n, z) + a(w^n, z), \end{aligned}$$

due to the orthogonality between V_{ms} and V_{f}. Rearranging the terms, we have

$$b(v^n, z) + b(w^n, z) = b(u_{\mathrm{lod}}^n, z) \approx 0.$$

That is, in the steady state phase, the solution becomes orthogonal with respect to B instead of A.

Localized version

The ideal method as currently stated is defined on the entire fine grid which is not computationally feasible. For this purpose we construct a localized multiscale space $V_{\mathrm{ms},k} := V_H - R_{\mathrm{f},k}V_H$ in complete analogy to the localization procedure in Section 3.1. For this localization to be valid it is required that each basis corrector $R_{\mathrm{f}}\lambda_x$ satisfies the same exponential decay as $\mathcal{Q}_{\mathrm{f}}\lambda_x$ from Section 3.1. However, we quickly note that $R_{\mathrm{f}}\lambda_x$ solves the same type of problem as $\mathcal{Q}_{\mathrm{f}}\lambda_x$ but with diffusion $A + \tau B$, and hence satisfies the required decay property by classical LOD theory.

With the space $V_{\mathrm{ms},k}$ defined, we are able to localize the computations corresponding to the system (4.1.5) by replacing the multiscale space by its localized counterpart. It remains to localize the computations of the fine-scale system in (4.1.6), which equivalently can be written as

$$a(\bar{\partial}_t w^n, z) + b(w^n, z) = \frac{1}{\tau} a(v^{n-1}, z).$$

We replace the right-hand side by its localized version $v_k^{n-1} \in V_{\mathrm{ms},k}$ and note that $v_k^{n-1} = \sum_{x\in\mathcal{N}} \alpha_x^{n-1}(\lambda_x - R_{\mathrm{f},k}\lambda_x)$. Thus, we seek our localized fine-scale solution as $w_k^n = \sum_{x\in\mathcal{N}} w_{k,x}^n$, where $w_{k,x}^n \in V_{\mathrm{f},k}^x$ solves

$$a(\bar{\partial}_t w_{k,x}^n, z) + b(w_{k,x}^n, z) = \frac{1}{\tau} a(\alpha_x^{n-1}(\lambda_x - R_{\mathrm{f},k}\lambda_x), z), \tag{4.1.7}$$

for all $z \in V_{\mathrm{f},k}^x$, so that the computation of this equation is localized to a patch surrounding the node $x \in \mathcal{N}$. We introduce the functions $\xi_{k,x}^\ell \in V_{\mathrm{f},k}^x$ as solution to the parabolic equation

$$a(\bar{\partial}_t \xi_{k,x}^\ell, z) + b(\xi_{k,x}^\ell, z) = \frac{1}{\tau} a(\chi_1(\ell)(\lambda_x - R_{\mathrm{f},k}\lambda_x), z), \tag{4.1.8}$$

for all $z \in V_{\mathrm{f},k}^x$ and $\ell = 1, 2, \ldots, N$ with initial value $\xi_{k,x}^0 = 0$. Here $\chi_1(\ell)$ denotes an indicator function that equals 1 when $\ell = 1$ and 0 otherwise. In Figure 4.1, the function $\xi_{k,x}^\ell$ for a fixed node $x \in \mathcal{N}$ is plotted. It holds that $w_{k,x}^n = \sum_{\ell=1}^n \alpha_x^{n-\ell}\xi_{k,x}^\ell$ is the solution to (4.1.7), which can be shown by simply inserting it and canceling terms (see Paper I for the details).

With the localization procedure established, we are set to define the proposed GFEM. It reads: find $u_{\mathrm{lod},k}^n = v_k^n + w_k^n$, where $v_k^n = \sum_{x\in\mathcal{N}} \alpha_x^n(\lambda_x - R_{\mathrm{f},k}\lambda_x)$ satisfies

$$\tau(\bar{\partial}_t^2 v_k^n, z) + a(v_k^n, z) + \tau b(v_k^n, z) = \tau(f^n, z) + a(u_{\mathrm{lod},k}^{n-1}, z), \tag{4.1.9}$$

for all $z \in V_{\mathrm{ms},k}$, and $w_k^n = \sum_{x\in\mathcal{N}} \sum_{\ell=1}^{n} \alpha_x^{n-\ell} \xi_{k,x}^{\ell}$, where $\xi_{k,x}^{\ell} \in V_{\mathrm{f},k}^{x}$ solves (4.1.8). The method can be summarized as follows:

1. Construct the multiscale space $V_{\mathrm{ms},k} := V_h - R_{\mathrm{f},k} V_H$. This includes solving a localized version of the (stationary) corrector problem (4.1.4) for each basis function $\{\lambda_x\}_{x\in\mathcal{N}}$.

2. Solve for the fine-scale correctors $\{\xi_{k,x}^{\ell}\}_{\ell=1}^{N}$. For this purpose, the localized (parabolic) problem (4.1.8) is solved for each coarse node $x \in \mathcal{N}$. For a fixed node, this corresponds to solving a localized problem on the fine scale in each time step.

3. Compute the solution by solving (4.1.9). Note that in each time step, we must construct $w_k^{n-1} = \sum_{x\in\mathcal{N}} \sum_{\ell=1}^{n-1} \alpha_x^{n-1-\ell} \xi_{k,x}^{\ell}$ and add it to the right-hand side.

To justify the fact that we localize the fine-scale equation, we furthermore require that the functions $\{\xi_x^{\ell}\}_{\ell=1}^{N}$ satisfy an exponential decay as well. The following theorem, proven in Paper I, provides this requirement.

Theorem 4.1.2. *For any node $x \in \mathcal{N}$, let $\xi_x^{\ell} \in V_{\mathrm{f}}$ be the solution to*

$$a(\bar{\partial}_t \xi_x^{\ell}, z) + b(\xi_x^{\ell}, z) = \frac{1}{\tau} a(\chi_1(\ell)(\lambda_x - R_{\mathrm{f}}\lambda_x), z),$$

for all $z \in V_{\mathrm{f}}$, with initial value $\xi_x^0 = 0$. Then there exist constants $c > 0$ and $C > 0$ such that for any $k \geq 1$

$$\|\xi_x^{\ell}\|_{H^1(D\setminus N^k(x))} \leq C e^{-ck} \|\lambda_x\|_{H^1},$$

for sufficiently small time step τ.

Error analysis

For the error analysis of this method the solution is first decomposed as $u_{\mathrm{lod}}^n = u_{\mathrm{lod},1}^n + u_{\mathrm{lod},2}^n$, where $u_{\mathrm{lod},1}^n$ has zero initial data and $u_{\mathrm{lod},2}^n$ has zero source data. The error of each decomposed part is then analyzed separately. We state the final result here and refer to Paper I where the full analysis is thoroughly investigated.

Theorem 4.1.3. *Let u_h^n and u_{lod}^n be the solutions to* (4.1.2) *and* (4.1.5)-(4.1.6)*, respectively. The solutions can be split into $u_h^n = u_{h,1}^n + u_{h,2}^n$ and $u_{\mathrm{lod}}^n = u_{\mathrm{lod},1}^n + u_{\mathrm{lod},2}^n$,*

where the first part has vanishing initial data, and the second part a vanishing right hand side. The errors are bounded by

$$\sum_{j=2}^{n} \tau \|u_{h,1}^j - u_{\mathrm{lod},1}^j\|_{H^1(D)}^2 \leq CH^2 \left(\sum_{j=1}^{n} \tau (\|f^j\|^2 + \|\bar{\partial}_t f^j\|^2) + \max_{j=1,\dots,n} \|f^j\|^2 \right),$$

$$\sum_{j=2}^{n} \tau t_j^2 \|u_{h,2}^j - u_{\mathrm{lod},2}^j\|_{H^1(D)}^2 \leq CH^2 (\|\bar{\partial}_t u_h^1\|_{H^1(D)}^2 + \|u_h^1\|_{H^1(D)}^2 + \|u_h^0\|_{H^1(D)}^2),$$

for $n \geq 2$, where the constants are independent of variations in A and B, but depend on the upper and lower bounds of A and B.

Remark 4.1.4. The theorem states optimal order convergence for the ideal method, stated in (4.1.5)-(4.1.6). In the localized method (4.1.9), an additional error will appear due to the localization procedure. However, due to the exponential decay of the basis correctors $R_{\mathrm{f}}\lambda_x$ (see [53, Theorem 4.1]) and the fine-scale functions ξ_x^ℓ (by Theorem 4.1.2), it holds for $k \sim \log(1/H)$ that the difference between the ideal and localized method converges with higher order than the error in Theorem 4.1.3. For details on the localization error, we refer to [51].

Reduced basis approach

The proposed method as stated so far is promising, but it requires us to solve the fine-scale system (4.1.8) for each coarse node $x \in \mathcal{N}$ and for each time step. This quickly becomes computationally challenging as the final time T increases. We reduce the complexity of the method by applying a so-called *reduced basis method*. By doing so, it will suffice to find solutions for $M < N$ time steps, and use the computed information to approximate the remaining ones in a significantly cheaper and more efficient way.

As motivation for the reduced basis approach, we first note that the system (4.1.8) which $\xi_{k,x}^n$ satisfies is a parabolic-type problem with zero source. As discussed in Section 2.2, the solutions to such a system decay exponentially from their initial data, until they have completely vanished. To illustrate this effect, we fix $x \in \mathcal{N}$ and compute $\{\xi_{k,x}^n\}$ for $n = 1, 2, \dots, 200$. The functions are computed on the unit interval with time step $\tau = 0.01$ and coefficients

$$A(x) = \left(2 - \sin\left(\tfrac{2\pi x}{\varepsilon_A}\right)\right)^{-1} \text{ and } \quad B(x) = \left(2 - \cos\left(\tfrac{2\pi x}{\varepsilon_B}\right)\right)^{-1},$$

with $\varepsilon_A = 2^{-4}$ and $\varepsilon_B = 2^{-6}$, where k is chosen so that the support covers the

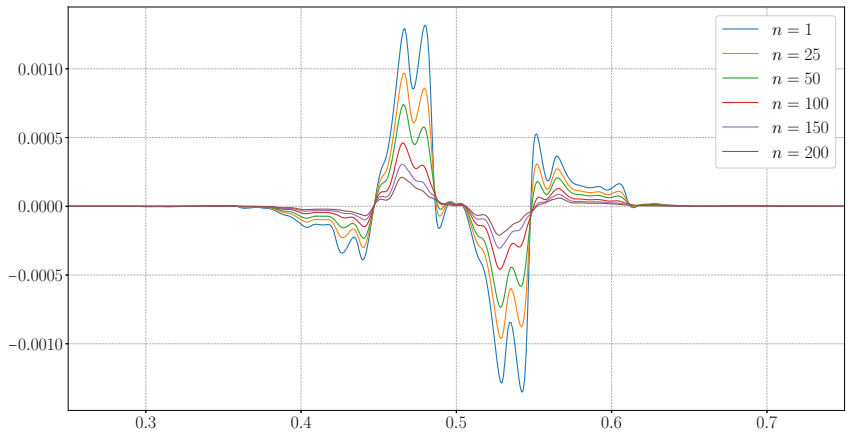

Figure 4.1: Illustration of a fine-scale corrector function $\xi_{k,x}^n$ vanishing with increasing time step n.

whole interval. Figure 4.1 displays the function $\xi_{k,x}^n$ for the selected time steps $n = 1, 25, 50, 100, 150, 200$.

While Figure 4.1 illustrates the rapid decay well, it is moreover important to note that the function $\xi_{k,x}^n$ maintains a similar shape through all time steps. This suggests that it is possible to evaluate the solutions for only a few time steps, and utilize their information to determine the remaining functions. To further investigate this idea, we analyze the singular values of the computed solutions $\{\xi_{k,x}^n\}_{n=1}^N$. The singular values are plotted in Figure 4.2 in the case $N = 100$. Here, we observe that the values decrease rapidly, with most of them falling within the machine precision level. In practice, this means that it is possible to compute the information for all of $\{\xi_{k,x}^n\}_{n=1}^N$ from just a few $\xi_{k,x}^n$. This property can be exploited to lower the computational complexity by employing a reduced basis method.

The idea behind reduced basis methods is to use the information from M number of pre-computed solutions to construct a low-dimensional space $V_{M,k,x}^{\mathrm{RB}}$, in which approximate solutions can be computed efficiently. The approach applied to compute an approximation of the set $\{\xi_{k,x}^n\}_{n=1}^N$ is as follows.

1. Pick $M \ll N$, and compute $\{\xi_{k,x}^n\}_{n=1}^M$ by (4.1.8).
2. Orthonormalize $\{\xi_{k,x}^n\}_{n=1}^M$ using, e.g., Gram–Schmidt orthonormalization. This yields a set of orthonormal vectors $\{\zeta_{k,x}^n\}_{n=1}^M$, called the *reduced basis*.

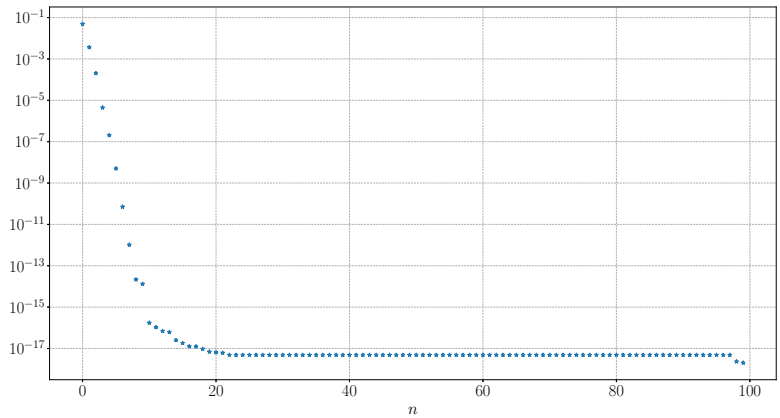

Figure 4.2: The singular values computed by singular value decomposition of the matrix composed by $\{\xi_{k,x}^n\}_{n=1}^{100}$. Note that after the first $\sim$10 singular values, the remaining ones lie on the machine precision level.

3. Construct the *reduced basis space* $V_{M,k,x}^{\mathrm{RB}} := \mathrm{span}(\{\zeta_{k,x}^n\}_{n=1}^M)$.

4. Compute the approximate solutions $\{\xi_{k,x}^{n,\mathrm{rb}}\}_{n=M+1}^N$ using (4.1.8), with the full space $V_{\mathrm{f},k}^x$ replaced by the low-rank space $V_{M,k,x}^{\mathrm{RB}}$.

Note that computing an approximate solution $\xi_{k,x}^{n,\mathrm{rb}} \in V_{M,k,x}^{\mathrm{RB}}$ is reduced to solving an $M \times M$ matrix system. That is, while computing the M first solutions can be challenging, solving for the $N - M$ remaining functions is significantly cheaper. Moreover, we remark that the analysis in Paper I does not include the error from the reduced basis approximations. However, the theory on reduced basis techniques is well-established, and the reader is referred to [60] for an introduction to the field.

We conclude the section by providing numerical examples illustrating the convergence rate of the proposed method, as well as the error introduced by the reduced basis approach. Before this, we quickly summarize the method and remark on the computational complexity. At first, the proposed method constructs $V_{\mathrm{ms},k}$ by solving linear systems on the localized fine scale for each coarse basis function. In turn, we compute $\{\xi_{k,x}^n\}_{n=1}^M$ by solving a localized fine-scale system N_H times for M time steps. This yields the space $V_{M,k,x}^{\mathrm{RB}}$ for each node $x \in \mathcal{N}$. The remaining approximations $\{\xi_{k,x}^{n,\mathrm{rb}}\}_{n=M+1}^N$ are found by solving $N - M$ number of $M \times M$ matrix systems. Finally, the solution, denoted $u_{\mathrm{lod},k}^{N,\mathrm{rb}}$, is computed on the coarse grid with multiscale space $V_{\mathrm{ms},k}$.

Numerical examples

Consider a unit square domain $D = [0,1] \times [0,1]$, and coefficients A and B with randomly generated values in the interval $[10^{-1}, 10^3]$ varying on the scale $\varepsilon = 2^{-6}$. For the system data, the initial values are set to zero and the source to $f \equiv 1$. The final time is set to $T = 1$ and the temporal domain is discretized with $\tau = 0.02$.

First, we compute the error between the localized method (without the reduced basis approach) and a reference solution computed on the fine grid. This is done for coarse mesh sizes $H = 2^{-i}$, $i = 1, \ldots, 5$ with localization parameter $k = \log_2(1/H)$. The relative error in $H^1(D)$-norm is plotted, and displayed in Figure 4.3. For comparison, the error for the standard FEM is also included, as well as the standard LOD method when correcting the basis functions only using A or B, respectively. Here, we see how neither FEM nor the standard LOD method suffices, while the proposed method achieves optimal order convergence instantly.

As a second example, we analyze the error that arise from the reduced basis approach. We fix the coarse mesh size to $H = 2^{-5}$, and plot the error as functions of the number of pre-computed solutions M used to construct the reduced basis. This is illustrated in Figure 4.4. Note that approximately $M = 10$ pre-computed solutions suffices in the case $H = 2^{-5}$ for the reduced basis approach to not perturb the convergence rate of the method.

4.2 Parabolic equation with time-dependent diffusion

The second case we consider for the extension of the LOD framework is the parabolic equation of the form

$$\begin{aligned} \dot{u} - \nabla \cdot (A \nabla u) &= f, \quad \text{in } D \times (0,T], \\ u &= 0, \quad \text{on } \partial D \times (0,T], \\ u(0) &= 0, \quad \text{in } D, \end{aligned} \tag{4.2.1}$$

where $T > 0$ and D is a polygonal (or polyhedral) domain in $\mathbb{R}^d$, $d = 2, 3$. In contrast to the parabolic case dealt with in [50], we have $A = A(t, x)$ with rapid oscillations in both time and space. We remark that the choice of zero initial data is made to simplify the presentation of our proposed method, and that nonzero data can be considered with just a few alterations. The parabolic equa-

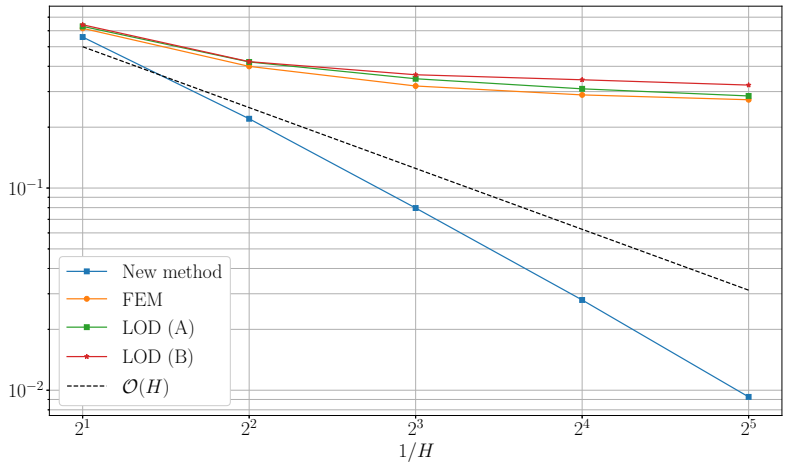

Figure 4.3: The relative $H^1(D)$-error $\|u_h^N - u_{\mathrm{lod},k}^N\|_{H^1(D)}/\|u_h^N\|_{H^1(D)}$ between the reference solution and the approximate solution computed with the proposed GFEM (excluding the reduced basis approach).

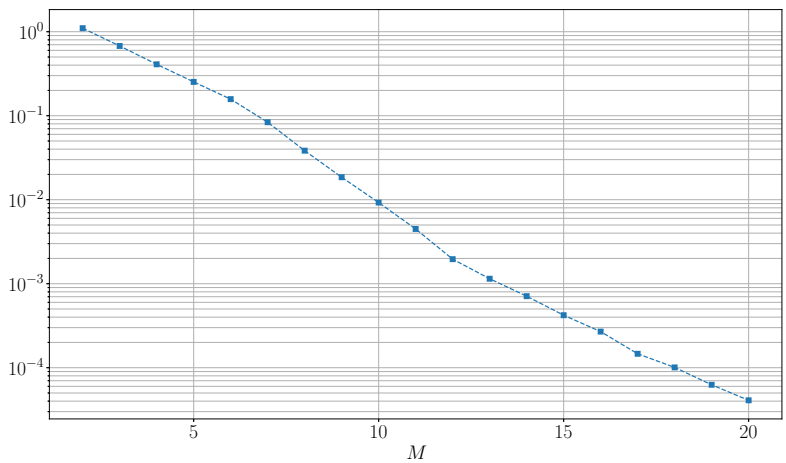

Figure 4.4: The relative $H^1(D)$-error $\|u_{\mathrm{lod},k}^N - u_{\mathrm{lod},k}^{N,\mathrm{rb}}\|_{H^1(D)}/\|u_{\mathrm{lod},k}^N\|_{H^1(D)}$ for the proposed GFEM with and without the reduced basis approach, as function of the number of pre-computed solutions used for the reduced basis.

tion (4.2.1) appears in several real life applications, where common examples include heat transfer and modeling of pressure in compressible flow [62, 45, 31]. In particular, the time-dependency in the diffusion is highly relevant when considering a heat conductor undertaking radioactive decay [68]. Furthermore, a parabolic problem posed on a time-dependent domain can be mapped to a problem posed on a fixed domain with time-dependent coefficients.

Weak form and finite elements

We begin by deriving the weak formulation of (4.2.1), and its corresponding finite element formulation. Let $L^2(0,T;\mathcal{B})$ and $H^1(0,T;\mathcal{B})$ be the standard Bochner spaces with norm

$$\|v\|_{L^2(0,T;\mathcal{B})} = \left(\int_0^T \|v\|_{\mathcal{B}}^2 \,\mathrm{d}t\right)^{1/2},$$
$$\|v\|_{H^1(0,T;\mathcal{B})} = \left(\int_0^T \|v\|_{\mathcal{B}}^2 + \|\dot{v}\|_{\mathcal{B}}^2 \,\mathrm{d}t\right)^{1/2},$$

where $\mathcal{B}$ is a Banach space with norm $\|\cdot\|_{\mathcal{B}}$. Throughout this section, we abbreviate the Bochner spaces by omitting the interval and the domain and write, e.g., $L^2(H_0^1) := L^2(0,T;H_0^1(D))$. We consider the following weak space-time formulation: find $u \in V_{\mathrm{tr}} := L^2(H_0^1) \cap H^1(H^{-1})$ such that

$$\int_0^T \langle \dot{u}, v\rangle + a(t;u,v)\,\mathrm{d}t = \int_0^T \langle f, v\rangle \,\mathrm{d}t \tag{4.2.2}$$

for all $v \in V_{\mathrm{te}} := L^2(H_0^1)$. Here, we have denoted by $\langle\cdot,\cdot\rangle$ the dual pairing of $H^{-1}(D)$ and $H_0^1(D)$. Moreover, the bilinear form $a(t;\cdot,\cdot)\colon H_0^1(D)\times H_0^1(D) \to \mathbb{R}$ is defined by

$$a(t;v,w) := \int_D A(t,\cdot)\nabla v \cdot \nabla w \,\mathrm{d}x$$

for almost all $t \in (0,T)$. From here on, we omit the t-dependence and abbreviate $a(\cdot,\cdot) := a(t;\cdot,\cdot)$.

We begin by introducing the space-time discretization on the fine scale. Let V_h be defined as in Section 2.1 for the spatial part. For the temporal discretization, we introduce the fine time step τ and set $t_i = i\tau$, $i = 1,\dots,N_\tau$ as the uniform partition with $t_{N_\tau} = T$. Denote by $\mathcal{I}_\tau$ the decomposition of $[0,T]$ into sub-intervals $[t_{i-1},t_i]$, $i = 1,\dots,N_\tau$. With respect to this discretization, we introduce two discrete spaces $\hat{V}_\tau$ and V_τ as the temporal trial and test space

respectively, defined by

$$\hat{V}_\tau := \{v \in H^1(0,T) : \ v|_I,\ I \in \mathcal{I}_\tau,\ \text{is a polynomial of degree } \leq 1, v(0) = 0\},$$
$$V_\tau := \{v \in L^2(0,T) : \ v|_I,\ I \in \mathcal{I}_\tau,\ \text{is constant}\}.$$

Based on the above definitions of spatial and temporal spaces, we introduce corresponding tensor-product space-time finite element spaces with respect to the full domain $[0,T] \times D$. We set

$$\hat{V}_{h,\tau} := \hat{V}_\tau \times V_h, \qquad V_{h,\tau} := V_\tau \times V_h$$

as trial and test space, respectively. The finite element formulation of (4.2.2) now states: find $u_{h,\tau} \in \hat{V}_{h,\tau}$ such that

$$\int_0^T \langle \dot{u}_{h,\tau}, v_{h,\tau} \rangle + a(u_{h,\tau}, v_{h,\tau}) \, \mathrm{d}t = \int_0^T \langle f, v_{h,\tau} \rangle \, \mathrm{d}t$$

for all $v_{h,\tau} \in V_{h,\tau}$. Note that, for the parabolic problem, we base our finite element problem on a Petrov–Galerkin ansatz, i.e., the trial and test spaces do not coincide.

Space-time multiscale method

For our space-time multiscale method we will, in similarity to previous LOD based methods, introduce corresponding coarse spaces. For the spatial discretization, define V_H and the interpolant $I_H = E_H \circ \Pi_H$ as in Section 3.1, and let $\{\varphi_x\}_{x \in \mathcal{N}_H}$ denote the standard finite element basis functions for V_H. For the temporal discretization, let $\mathcal{T} > 0$ be a coarse time step, and let $T_i = i\mathcal{T}$, $i = 0, 1, \ldots, N$. Denote by $\mathcal{I}_\mathcal{T}$ the decomposition of the time interval $[0,T]$ into sub-intervals $[T_{i-1}, T_i]$, $i = 1, \ldots, N$ of uniform size with $T_N = T$. Then, in analogy with the fine temporal spaces, we define $\hat{V}_\mathcal{T}$ and $V_\mathcal{T}$ as coarse temporal trial and test spaces based on the decomposition $\mathcal{I}_\mathcal{T}$. Moreover, let $\{\zeta_i\}_{i=1}^N$ denote the piecewise linear basis functions that span $\hat{V}_\mathcal{T}$, and $\{\chi_i\}_{i=1}^N$ the piecewise constant basis functions that span $V_\mathcal{T}$, where $\chi_i = \mathbb{1}_{[T_{i-1},T_i]}$. The coarse space-time spaces are then set as $\hat{V}_{H,\mathcal{T}} := \hat{V}_\mathcal{T} \times V_H$ as trial space, and $V_{H,\mathcal{T}} := V_\mathcal{T} \times V_H$ as test space.

Next, use the spatial interpolant to define the remainder spaces

$$\hat{W}_{h,\tau} := \Big\{ w \in \hat{V}_{h,\tau} : \; I_H w(T_i, \cdot) = 0 \text{ for all } i = 0, \dots, N \Big\},$$
$$W_{h,\tau} := \Big\{ w \in V_{h,\tau} : \; \mathcal{T}^{-1} \int_{T_{i-1}}^{T_i} I_H w \, \mathrm{d}t = 0 \text{ for all } i = 1, \dots, N \Big\},$$

which we will use as our fine trial and test spaces respectively. Note that, by construction, $\hat{V}_{h,\tau} = \hat{V}_{H,\mathcal{T}} \oplus \hat{W}_{h,\tau}$ and $V_{h,\tau} = V_{H,\mathcal{T}} \oplus W_{h,\tau}$.

Our proposed space-time multiscale method is based on the variational multiscale method, first introduced in [30], and aims to extend the LOD framework to space- and time-dependent coefficients. The main idea is to decompose the solution into a coarse part in $\hat{V}_{H,\mathcal{T}}$ and a remainder part in $\hat{W}_{h,\tau}$ and then consider (4.2.2) for test functions in the coarse test space $V_{H,\mathcal{T}}$ and the fine test space $W_{h,\tau}$ separately. In turn, this yields a coarse-scale and a fine-scale equation respectively. The main purpose of the fine-scale equation is to compute certain *correctors*, which we utilize to enrich the coarse-scale equation with the fine-scale behavior of the diffusion. The proposed method reads: find $\tilde{u}_{H,\mathcal{T}} = u_{H,\mathcal{T}} + \mathcal{Q} u_{H,\mathcal{T}} \in (1 + \mathcal{Q}) \hat{V}_{H,\mathcal{T}}$ such that $u_{H,\mathcal{T}} \in \hat{V}_{H,\mathcal{T}}$ solves

$$\int_0^T \langle \tfrac{\mathrm{d}}{\mathrm{d}t} (1 + \mathcal{Q}) u_{H,\mathcal{T}}, v_{H,\mathcal{T}} \rangle + a((1 + \mathcal{Q}) u_{H,\mathcal{T}}, v_{H,\mathcal{T}}) \, \mathrm{d}t = \int_0^T \langle f, v_{H,\mathcal{T}} \rangle \, \mathrm{d}t, \tag{4.2.3}$$

for all $v_{H,\mathcal{T}} \in V_{H,\mathcal{T}}$ and $\mathcal{Q} u_{H,\mathcal{T}} \in \hat{W}_{h,\tau}$ solves

$$\int_0^T \langle \tfrac{\mathrm{d}}{\mathrm{d}t} \mathcal{Q} u_{H,\mathcal{T}}, w_{h,\tau} \rangle + a(\mathcal{Q} u_{H,\mathcal{T}}, w_{h,\tau}) \, \mathrm{d}t = - \int_0^T \langle \dot{u}_{H,\mathcal{T}}, w_{h,\tau} \rangle + a(u_{H,\mathcal{T}}, w_{h,\tau}) \, \mathrm{d}t \tag{4.2.4}$$

for all $w_{h,\tau} \in W_{h,\tau}$. Due to linearity, we may take (4.2.4) and further decompose it into corrector problems with local space-time basis functions $\Lambda_x^j := \zeta_j \varphi_x \in \hat{V}_{H,\mathcal{T}}$ as source, where $j \in \{1, \dots, N\}$ denotes the temporal node and $x \in \mathcal{N}$ the spatial node that the basis function corresponds to. That is, we define a corrector $\mathcal{Q} \Lambda_x^j \in \hat{W}_{h,\tau}$ as the solution to

$$\int_0^T \langle \tfrac{\mathrm{d}}{\mathrm{d}t} \mathcal{Q} \Lambda_x^j, w_{h,\tau} \rangle + a(\mathcal{Q} \Lambda_x^j, w_{h,\tau}) \, \mathrm{d}t = - \int_0^T \langle \dot{\Lambda}_x^j, w_{h,\tau} \rangle + a(\Lambda_x^j, w_{h,\tau}) \, \mathrm{d}t \tag{4.2.5}$$

for all $w_{h,\tau} \in W_{h,\tau}$, with initial condition $\mathcal{Q} \Lambda_x^j(0, \cdot) = 0$. Note that, due to $\operatorname{supp}(\Lambda_x^j) = [T_{j-1}, T_{j+1}] \times N(x)$ and the initial condition in (4.2.5), the integrals are immediately reduced from $[0, T]$ to $[T_{j-1}, T]$. Without loss of generality, we will therefore restrict the presentation to the case $j = 1$ and abbreviate

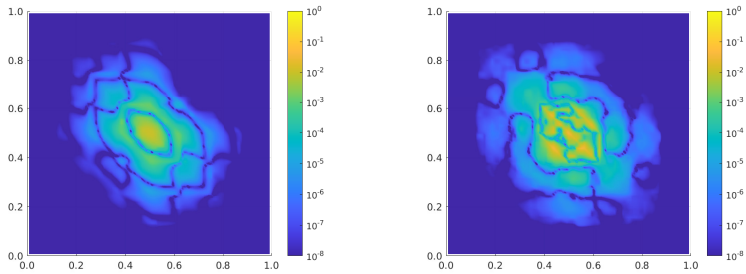

(a) $\mathcal{Q}\Lambda(\tau, \cdot)$ **(b)** $\mathcal{Q}\Lambda(T_1 + \tau, \cdot)$

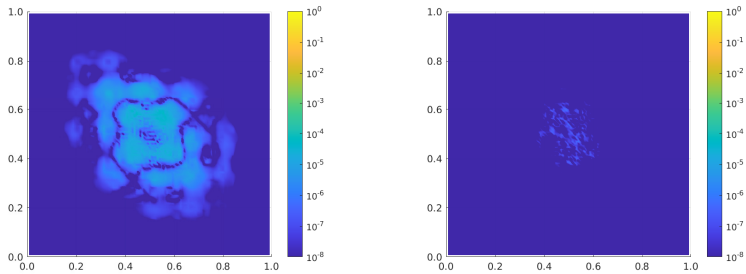

(c) $\mathcal{Q}\Lambda(T_2 + \tau, \cdot)$ **(d)** $\mathcal{Q}\Lambda(T_3 + \tau, \cdot)$

Figure 4.5: Space-time decay of a basis corrector $\mathcal{Q}\Lambda$ in logarithmic scale.

$\Lambda := \Lambda_x^1$, $\zeta := \zeta_1$, and $\varphi := \varphi_x$. We emphasize that (4.2.5) is a corrector problem which can be compared to that of (3.1.3) for the standard LOD, but posed on the space-time domain. In a similar fashion, the correction $\mathcal{Q}\Lambda$ decays rapidly outside of the support of Λ, which is restricted in both space and time. This property is later exploited to localize the computations in both space and time. For an illustration of the function $\mathcal{Q}\Lambda$ and its decay, see Figure 4.5.

We wish to solve the system (4.2.5) without explicitly computing the fine-scale spaces $\hat{W}_{h,\tau}$ and $W_{h,\tau}$. Hence, we reformulate (4.2.5) as a constraint problem posed in the full discrete space $\hat{V}_{h,\tau}$ and with test functions in $V_{h,\tau}$. That is, let $\psi \in \hat{V}_{h,\tau}$ be the solution of

$$\begin{aligned} \int_0^T \langle \dot{\psi}, v \rangle + a(\psi, v)\,\mathrm{d}t + \sum_{i=1}^{N} \int_{T_{i-1}}^{T_i} \langle \lambda_i, I_H v \rangle\,\mathrm{d}t &= -\int_0^T \langle \dot{\Lambda}, v \rangle + a(\Lambda, v)\,\mathrm{d}t \\ \sum_{j=1}^{N} \langle I_H \psi(T_j), \mu_j \rangle &= 0, \end{aligned} \tag{4.2.6}$$

for all $v \in V_{h,\tau}$, $\mu_j \in V_H$, $j = 1, \dots, N$, where $(\lambda_1, \dots, \lambda_N) \in V_H \times \dots \times V_H$ are the associated Lagrange multipliers. Note that, by construction, (4.2.5) and (4.2.6) are equivalent, i.e., $\mathcal{Q}\Lambda = \psi$.

Error of the ideal method

The method presented in (4.2.3)-(4.2.4) is referred to as our ideal method. For the corresponding error estimate, we introduce the norms for the trial and test space respectively as

$$\|v\|_{V_{\mathrm{tr}}}^2 := \int_0^T \|\nabla \overline{v}(t,\cdot)\|_{L^2(\Omega)}^2 + \|\dot{v}(t,\cdot)\|_{H^{-1}(D)}^2 \,\mathrm{d}t + \|v(T)\|_{L^2(D)}^2,$$
$$\|v\|_{V_{\mathrm{te}}}^2 := \int_0^T \|\nabla v(t,\cdot)\|_{L^2(\Omega)}^2 \,\mathrm{d}t,$$

where $\overline{v} := \sum_{i=1}^{N_\tau} \left(\tau^{-1} \int_{t_{i-1}}^{t_i} v(s,\cdot)\,\mathrm{d}s\right) \chi_i$ is the mean with respect to the fine temporal discretization. These norms are essential for the analysis of certain space-time Petrov–Galerkin discretizations as in [65] on which our approach relies. The error for the proposed ideal method is then quantified by following theorem, which is proven in Paper II.

Theorem 4.2.1 (Error of the ideal method)**.** *Assume that the right-hand side fulfills $f \in L^2(L^2) \cap H^1(H^{-1})$. Then the error between the solutions $u_{h,\tau}$ and $\tilde{u}_{H,\mathcal{T}}$ satisfies*

$$\|\tilde{u}_{H,\mathcal{T}} - u_{h,\tau}\|_{V_{\mathrm{tr}}} \leq C\,(H + \mathcal{T})\,\|f\|_{L^2(L^2)\cap H^1(H^{-1})}.$$

Localization in time and space

Theorem 4.2.1 states that our novel method converges with optimal order. However, similarly to earlier LOD based methods, the formulation as currently stated is ideal, but impractical. The method is based on auxiliary corrector problems defined on the entire fine space-time grid, which is not computationally feasible, as earlier discussed. To circumvent this issue, one observes that a corrector function ψ decays exponentially fast away from the support of the underlying basis function Λ. Without a great impact on the approximation property, it is therefore possible to restrict the fine-scale computations to local spatial patches as for the standard LOD, and to a limited number of coarse time steps, yielding a localized method in both space and time. For the temporal localization, we begin by demonstrating how the basis corrector ψ is computed by a sequential approach. This turns into an efficient scheme whose computa-

tions easily can be restricted in time. We emphasize that the basis correctors are independent, which makes parallelization possible in both space and time.

To define the sequential approach, we begin by dividing the integral in (4.2.6) into local integrals over $[T_{j-1}, T_j]$, $j = 1, \dots, N$ and define for given j the local version of $\hat{V}_{h,\tau}$ by

$$\hat{V}_{h,\tau}^j := \{v|_{[T_{j-1},T_j]\times D} : \, v \in V_{h,\tau}\}.$$

Further, we denote with $\xi_j \in \hat{V}_{h,\tau}^j$, $\xi_j(T_{j-1}) = 0$ the solution of

$$\begin{aligned} \int_{T_{j-1}}^{T_j} \langle \dot{\xi}_j, v\rangle + a(\xi_j, v) + \langle \lambda_j, I_H v\rangle \,\mathrm{d}t = -\int_{T_{j-1}}^{T_j} \langle \dot{\Lambda}, v\rangle + a(\Lambda, v) \\ - \langle \tfrac{1}{T}\xi_{j-1}(T_{j-1}), v\rangle \\ + a(\tfrac{T_j - t}{T}\xi_{j-1}(T_{j-1}), v)\,\mathrm{d}t, \\ \langle I_H \xi_j(T_j), \mu\rangle = 0, \end{aligned} \tag{4.2.7}$$

for all $v \in V_{h,\tau}$, $\mu \in V_H$, where $\lambda_j \in V_H$ is the associated Lagrange multiplier. For $j = 1$, we explicitly set $\xi_0(T_0) = 0$ such that the third and the fourth term on the right-hand side of (4.2.7) vanish. Note that the functions $\{\xi_j\}_{j=1}^N$ are constructed in a way such that

$$\psi = \sum_{j=1}^{N} \big(\xi_j + \tfrac{T_j - t}{T}\xi_{j-1}(T_{j-1})\big)\mathbb{1}_{[T_{j-1},T_j]}.$$

We emphasize that the basis function Λ only has support on the first two coarse intervals. That is, for $j > 2$ the first two terms in (4.2.7) (and also in (4.2.6)) disappear and, consequently, ψ will begin to decay due to the parabolic nature of the problem.

Due to the decay property of ψ, there will be an $\ell \in \mathbb{N}$ such that for $j > \ell$, the sequential functions ξ_j will be of negligible size compared to the error of the ideal method. Hence, it suffices to restrict the computations to $\{\xi_j\}_{j=1}^{\ell}$. That is, we define our temporally localized corrector function by $\psi_\ell = \psi\,\mathbb{1}_{[0,T_\ell]}$, where we refer to ℓ as the *temporal localization parameter*. We remark that simply restricting the computations will make ψ_ℓ discontinuous, and thus it will no longer be a function in $\hat{V}_{h,\tau}$. However, this can easily be circumvented by choosing

$$\psi_\ell = \psi\,\mathbb{1}_{[0,T_\ell]} + \tfrac{T_{\ell+1} - t}{T}\xi_\ell(T_\ell)\,\mathbb{1}_{[T_\ell,T_{\ell+1}]}.$$

It remains to apply the spatial localization procedure, which follows in similar-

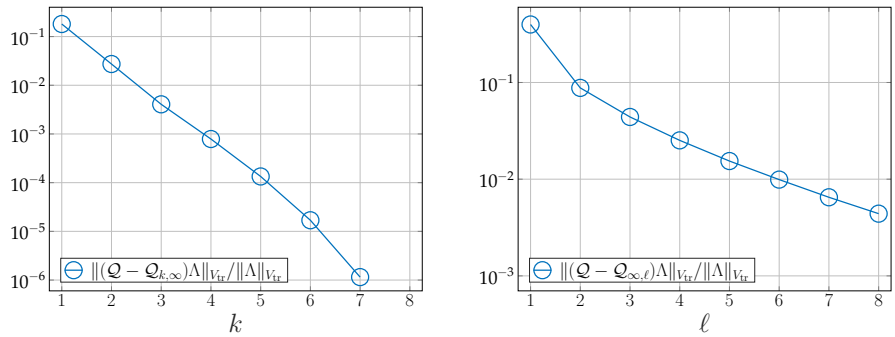

(a) Spatial decay. **(b)** Temporal decay.

Figure 4.6: The (relative) localization errors for a basis function Λ.

ity to Section 3.1. In total, this yields space-time localized basis functions, which we denote by $\mathcal{Q}_{k,\ell}$. The details of its specific construction is left to Paper II.

We conclude the discussion by numerically illustrating the space-time decay of a basis function Λ, which justifies the localization procedure. In Figure 4.5, the decay of a basis corrector in both space and time is depicted. Moreover, Figure 4.6 displays the error between an ideal basis function and its localized counterpart (in space and time, respectively) as a function of each respective localization parameter.

Final method

By applying the localization, we yield an efficient space-time multiscale method for which the convergence rate from Theorem 4.2.1 remains valid. The proposed *localized method* reads: find $\tilde{u}_{H,\mathcal{T},k,\ell} = u_{H,\mathcal{T},k,\ell} + \mathcal{Q}_{k,\ell}u_{H,\mathcal{T},k,\ell} \in (1+\mathcal{Q}_{k,\ell})\hat{V}_{H,\mathcal{T}}$ such that

$$\int_0^T \langle \tfrac{\mathrm{d}}{\mathrm{d}t}(1+\mathcal{Q}_{k,\ell})u_{H,\mathcal{T},k,\ell}, v_{H,\mathcal{T}}\rangle + a((1+\mathcal{Q}_{k,\ell})u_{H,\mathcal{T},k,\ell}, v_{H,\mathcal{T}})\,\mathrm{d}t = \int_0^T \langle f, v_{H,\mathcal{T}}\rangle\,\mathrm{d}t$$

for all $v_{H,\mathcal{T}} \in V_{H,\mathcal{T}}$. For this method, an a posteriori error has been derived with the same order of convergence as for the a priori error of the ideal method. We leave the details of the analysis to Paper II, and conclude with a numerical example illustrating the convergence of the error.

For the example, the diffusion A consists of randomly generated values in the interval $[0.01, 0.1]$ which are piecewise constant, varying with scales $\varepsilon_x = \varepsilon_t =$

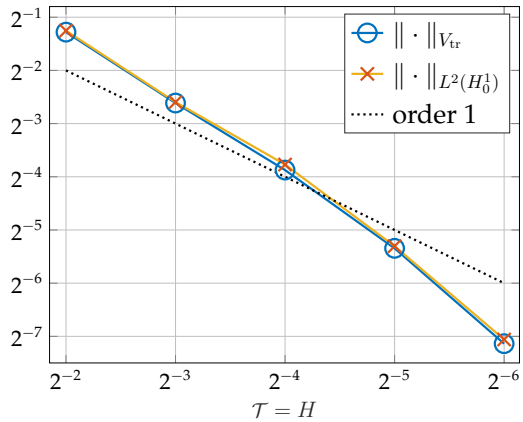

Figure 4.7: Relative error with respect to different space-time grid sizes $H = \mathcal{T}$.

2^{-5} in space and time. The fine mesh is defined by the parameters $h = \tau = 2^{-7}$ such that the variations in the coefficient are resolved. For the remaining problem data, we set the source to $f \equiv 1$ and the final time to $T = 1.25$. Localization in space is set to $k = \log_2(1/H)$, and in time we use $\ell = 4$ for all computations. The relative error is evaluated for the coarse parameters $H = \mathcal{T} = 2^{-i}$, $i = 2, \ldots, 6$. In Figure 4.7, the convergence rate for the problem is illustrated. It is seen how the proposed method satisfies linear convergence with respect to $H = \mathcal{T}$, which confirms the theoretical findings.

4.3 Wave equation on spatial networks

In this part, we model the propagation of elastic waves in fiber-based materials. Due to its intricate model, computations on the exact fiber network can be difficult. A so-called *spatial network model* simplifies the fiber network structure, thus lowering computational complexity and facilitating modeling challenges. More specifically, the network model approximates the three dimensional fiber cylinders by a web-like network, defined by nodes, edges, and edge weights, which together represent a discretized 1-D structure in $\mathbb{R}^d$. See Figure 4.8 for an illustrative example. This approach yields a discrete system, characterized by a symmetric, positive-definite matrix K whose data may inherit high variations from the network model. In [24], it was shown that model we analyze produce representable results in comparison to real-life paper simulations.

As model problem, we consider the discrete linear wave equation

$$\begin{aligned} MD_t^2 u + Ku &= Mf, \\ u(\cdot, 0) &= g, \\ D_t u(\cdot, 0) &= h, \end{aligned}$$

with corresponding weak form to find $u \in V$ such that

$$(MD_t^2 u, v) + (Ku, v) = (Mf, v), \tag{4.3.1}$$

for all $v \in V$, where K is related to a weighted graph Laplacian, M is a diagonal mass matrix, f the right-hand side data and $(\cdot, \cdot)$ the Euclidean scalar product. The discrete solution space V is defined in detail below. The goal is to efficiently compute an accurate coarse-scale approximation of the solution to (4.3.1). However, due to the network structure, the matrix K may inherit high variations in its data, which in turn affect the solution on the coarse scale. Moreover, unlike the the continuous PDE setting, the network does not have a natural coarse scale. To overcome these computational difficulties, we present a similar LOD approach to the one introduced for stationary equations in Section 3.1. We start by presenting the spatial network model and outlining the operators crucial to the approach.

Network definition and operators

The spatial network considered is represented by the connected graph $\mathcal{G} = (\mathcal{N}, \mathcal{E})$. Here, $\mathcal{N} \subset \mathbb{R}^d$ is a finite set of nodes, and

$$\mathcal{E} := \big\{\{x, y\} : \ x \text{ and } y \text{ are connected by an edge}\big\},$$

is an edge set consisting of unordered pairs of edges. In the following, if $\{x, y\} \in \mathcal{E}$, we refer to x and y as adjacent nodes, and denote this by $x \sim y$. The network is embedded into a spatial domain $D \subset \mathbb{R}^d$. For simplicity, we consider a hypercube domain, i.e., $D = [0, 1]^d$, and remark that more complicated domains can be considered with just a few alterations. Moreover, let $\Gamma \subseteq \partial D$ denote the (non-empty) set of nodes on the boundary to which a Dirichlet-type boundary condition is applied.

Let $\hat{V}$ be the space of real-valued functions defined on the node set $\mathcal{N}$, and let V be the corresponding space with imposed homogeneous boundary condition. That is,

$$V := \{v \in \hat{V} : v(x) = 0, \ x \in \Gamma\}.$$

For any subset $\omega \in D$, the set of nodes contained in ω is defined by $\mathcal{N}(\omega) := \mathcal{N} \cap \omega$. We further define the scalar product on $\hat{V}$ over the subset ω as

$$(u, v)_\omega := \sum_{x \in \mathcal{N}(\omega)} u(x)v(x),$$

with $(\cdot, \cdot) := (\cdot, \cdot)_D$.

We are now set to define the operators used in the model problem (4.3.1). Given a node $x \in \mathcal{N}$, define the diagonal linear operator $M_x : \hat{V} \to \hat{V}$ by

$$(M_x v, v) := \frac{1}{2} \sum_{y \sim x} |x - y| v(x)^2.$$

For any subdomain ω, we define $M_\omega := \sum_{x \in \mathcal{N}(\omega)} M_x$, and we frequently abbreviate $M := M_D$. Note that $(M_\omega 1, 1)$ can be interpreted as the mass of the network contained in ω. The operator M further defines a norm, namely $\left|v\right|_M := (Mv, v)^{1/2}$.

Let $L_x : \hat{V} \to \hat{V}$ be the reciprocal edge-length weighted graph Laplacian defined by

$$(L_x v, v) := \frac{1}{2} \sum_{y \sim x} \frac{\big(v(x) - v(y)\big)^2}{|x - y|},$$

and similarly define $L_\omega := \sum_{x \in \mathcal{N}(\omega)}$, with $L := L_D$. Note that this scaling corresponds to a 1D FEM stiffness matrix. The operator L is symmetric and positive semi-definite, and therefore defines a semi-norm $\left|v\right|_L := (Lv, v)^{1/2}$. Moreover, for the model problem (4.3.1), we use the symmetric and positive semi-definite linear operator $K : V \to V$. The operator K is assumed to be bounded and coercive with respect to the weighted graph Laplacian L. That is, it holds that

$$\alpha(Lv, v) \leq (Kv, v) \leq \beta(Lv, v), \tag{4.3.2}$$

where $0 < \alpha \leq \beta < \infty$. At last, K is assumed to be local, in the sense that $K = \sum_{x \in \mathcal{N}} K_x$, where each $K_x : \hat{V} \to \hat{V}$ is symmetric and positive semi-definite, with support on nodes adjacent to x. Note that since Γ is non-empty, and $\mathcal{G}$ is connected, it holds that L (and consequently K) is invertible. Furthermore, the operator K induces the norm $\left|v\right|_K := (Kv, v)^{1/2}$. An example

of an operator K that fulfills above assumptions is $K = \sum_{x\in\mathcal{N}} K_x$, where

$$(K_x v, v) := \frac{1}{2}\sum_{y\sim x} \gamma_{xy} \frac{\big(v(x) - v(y)\big)^2}{|x-y|}, \tag{4.3.3}$$

and $\gamma_{xy} \in (0,\infty)$ is a material parameter for the edge connecting x and y, e.g., heat conductivity. For this operator, the relation (4.3.2) holds with $\alpha := \min_{x,y\in\mathcal{N}} \gamma_{xy}$ and $\beta := \max_{x,y\in\mathcal{N}} \gamma_{xy}$. For more examples of operators K that satisfy the assumptions above, we refer to the work in [17, 23], as well as Paper III.

Network assumptions

Before defining the LOD extension, we require certain assumptions on the network. For this purpose, we begin by introducing boxes $B_R(x) \subset D$ of length $2R$, centered at $x = (x_1, \dots, x_d)$. These boxes will later be of importantance for the coarse-scale discretization of our method as well. To construct the boxes, we first let

$$\tilde{B}_R(x) := [x_1 - R, x_1 + R) \times \cdots \times [x_d - R, x_d + R),$$

and further define

$$B_R(x) := \tilde{B}_R(x) \cup \big(\overline{\tilde{B}_R(x)} \cup \partial D\big). \tag{4.3.4}$$

Note that, by construction, $B_R(x)$ does not contain its upper boundary in either dimension, unless it is a part of the global boundary ∂D. We are now prepared to state necessary properties for the network.

Assumptions 4.3.1 (Network properties)**.** *Let R_0 be a homogeneity parameter on the coarse-length scale. Then, the network satisfies following assumptions.*

1. *(Homogeneity). There is a uniformity parameter σ and a density parameter ρ such that*

   $$\rho \le (2R)^{-d} \big|1\big|^2_{M,B_R(x)} \le \sigma\rho$$

   holds, for all $R \ge R_0$ and all $x \in D$.

2. *(Connectivity). For all $R \ge R_0$, and all $x \in D$, there is a connected subgraph $\bar{\mathcal{G}} = \{\bar{\mathcal{N}}, \bar{\mathcal{E}}\}$ that contains*

   (a) all edges with at least one endpoint in $B_R(x)$, and

(b) no edges with at least one endpoint not in $B_{R+R_0}(x)$.

3. *(Locality). It holds that*

$$\max_{\{x,y\}\in\mathcal{E}} |x-y| < R_0,$$

i.e., all edge lengths are smaller than R_0.

4. *(Boundary density). For any boundary node $y \in \Gamma$, there exists $x \in \Gamma$ such that $|x-y| < R_0$.*

All together, the assumptions ensure that the considered network follows some basic guidelines. For instance, under the assumption of homogeneity, the density of a small part of the network (on the R_0-scale) must be comparable to the density of the network across the entire domain D. Furthermore, the locality assumption prevents edges from connecting over distances greater than R_0 within the network. At last, the connectivity property implies that the network, on the R_0-scale, is sufficiently connected. The connectivity assumption can also be used to derive certain inequalities valid on the network, such as analogous counterparts of Friedrichs and Poincaré inequalities. These inequalities are useful in the derivation of stability of interpolation onto the network, which is crucial for the LOD method. For more discussion on the assumptions, and in particular the connectivity, we refer to [17, Section 3].

Coarse-scale definition

The foundation of the LOD method is based on the decomposition of the solution space into a coarse-scale and a fine-scale part, respectively. In the standard PDE setting (see Section 3.1), the coarse and fine scales appear naturally from nested finite element spaces. For the spatial network setting, the definition of a coarse scale is less straight-forward. In [17, 23], the authors tackle this challenge by proposing an artificial coarse scale with minimal constraints on its relationship to the network.

Following the approach of [17, 23], we introduce a coarse finite element mesh of square shaped elements. More precisely, we begin by considering the boxes $B_R(x)$, defined in (4.3.4). Then, we define $\mathcal{T}_H$ as the family of partitions of D into hypercubes of length $H = 2^{-j}$, $j \in \mathbb{N}$, i.e.,

$$\mathcal{T}_H := \{B_{H/2}(x) : x = (x_1, \dots, x_d) \in D \text{ and } H^{-1}x_i + 1/2 \in \mathbb{N},\ i = 1, \dots, d\}.$$

Next, we introduce a first-order finite element space on the mesh $\mathcal{T}_H$. Let $\hat{Q}_H$ be

the space of continuous functions on D which, restricted to $T \in \mathcal{T}_H$, are linear combinations of the polynomials $z = (z_1, \ldots, z_d) \mapsto z^\alpha$ for the multi-index $\alpha = (\alpha_1, \ldots, \alpha_d)$, with $\alpha_i \in \{0, 1\}$. For instance, in the case $d = 2$, the space $\hat{Q}_H$ corresponds to the space of bilinear functions on $\mathcal{T}_H$. Furthermore, we define

$$Q_H := \{q \in \hat{Q}_H : q\big|_\Gamma = 0\}$$

as the associated finite element space fulfilling the Dirichlet boundary condition. Furthermore, we wish to restrict these spaces to nodes in D. Therefore, define $\hat{V}_H$ as the space of functions in $\hat{Q}_H$ restricted to $\mathcal{N}$, and similarly for V_H.

We conclude the part on the spatial discretization by defining a basis for the above constructed spaces. Denote by $\{y_i\}_{i=1}^m$ the nodes in $\mathcal{T}_H$, and let $\{\hat{\lambda}_i\}_{i=1}^m$ be the standard Lagrange finite element basis functions that span $\hat{Q}_H$. Furthermore, by $\{\lambda_i\}_{i=1}^m$ we denote the restrictions of $\{\hat{\lambda}_i\}_{i=1}^m$ to the network nodes, such that $\hat{V}_H = \text{span}(\{\lambda_i\}_{i=1}^m)$. Without loss of generality, we assume the space Q_H to be spanned by the $m_0 < m$ first basis functions, $\{\hat{\lambda}_i\}_{i=1}^{m_0}$. In Figure 4.8, a summary of the discretization process from initial network to final mesh $\mathcal{T}_H$ is illustrated.

Network interpolant

With the coarse finite element space V_H defined over the spatial network, we are now set to introduce the interpolant required for the decomposition of spaces. We define the following discrete interpolant inspired by the Scott–Zhang interpolant, initially presented in [63].

Definition 4.3.2. *Given a basis function λ_j, let T_j denote the (unique) corresponding element containing y_j, and define $\psi_j \in \hat{V}_H$ by the relation $(M_{T_j}\psi_j, \lambda_i) = \delta_{ij}$. The interpolant $I_H : V \to V_H$ is then defined as*

$$I_H v := \sum_{j=1}^{m_0} (M_{T_j}\psi_j, v)\varphi_j.$$

For this interpolant, one can show an interpolation estimate similar to (3.1.2). Indeed, in [17], it is shown that if Assumptions 4.3.1 are fulfilled, then I_H satisfies the estimate

$$H^{-1}\big|v - I_H v\big|_M + \big|I_H v\big|_L \leq C\big|v\big|_L,$$

for any function $v \in V$.

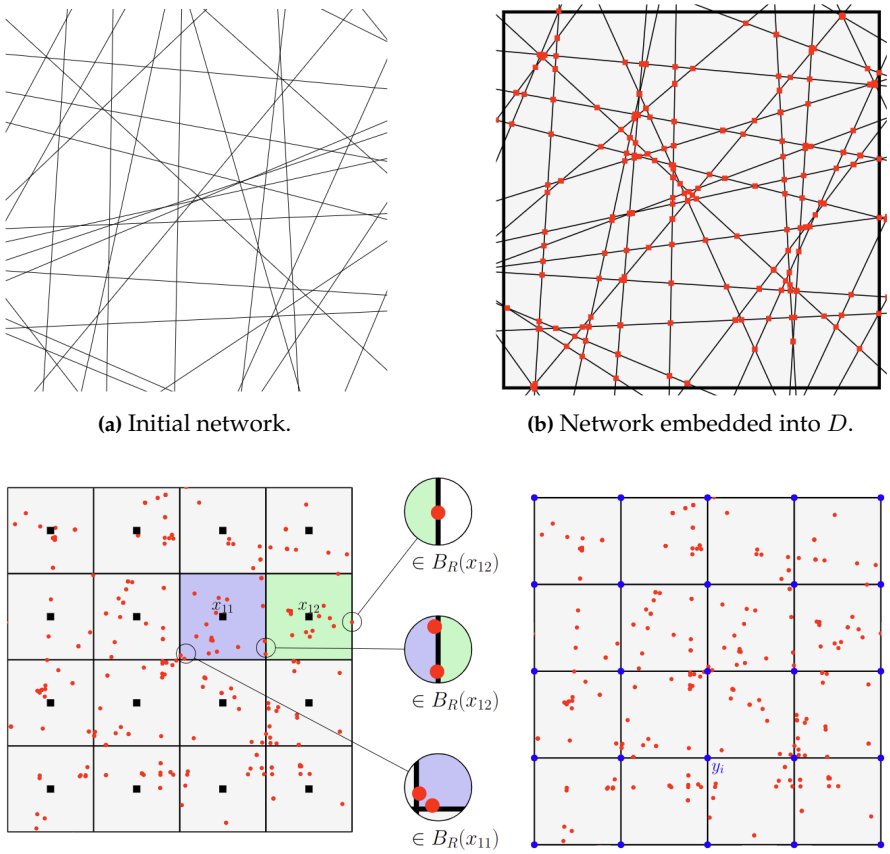

(a) Initial network.

(b) Network embedded into D.

(c) Boxes introduced.

(d) Final mesh.

Figure 4.8: Depiction of the discretization workflow from the initial network structure to a coarse- and fine-scale. In (a), the initial network is displayed. The network is then embedded into the spatial domain D, here set to a unit square. This is illustrated in (b), where the red nodes represent the node set $\mathcal{N}$ of the graph. In (c), the boxes $B_R(x)$ are introduced. Here, it is moreover shown how boundary nodes belong to a specific element. The final mesh $\mathcal{T}_H$ with coarse grid nodes $\{y_i\}_{i=1}^m$ (blue) is shown in (d), with the fine scale nodes (red) included.

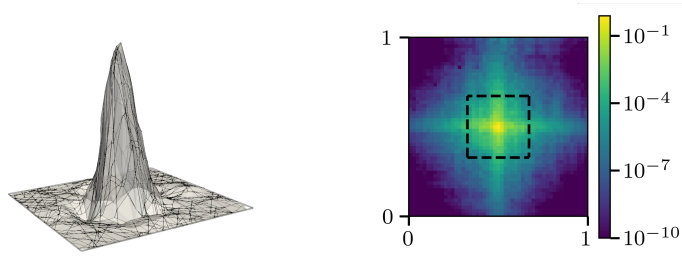

Figure 4.9: A modified basis function $\mathcal{Q}\lambda_i$ and its decay illustrated in logarithmic scale.

The LOD method on spatial networks

We are now set to construct an LOD based approach applicable to spatial network models. The interpolant I_H captures the coarse-scale behavior of functions, while the fine-scale features are recovered in the space $V_{\mathrm{f}} := \ker(I_H)$. On this space, we can define a corrector problem in similarity to the standard LOD method, but replacing the bilinear form $a(\cdot,\cdot)$ with the scalar-product $(K\cdot,\cdot)$. That is, we define $\mathcal{Q} : V \to V_{\mathrm{f}}$ such that

$$(K\mathcal{Q}v, w) = (Kv, w), \tag{4.3.5}$$

holds for all $v \in V_{\mathrm{f}}$. The multiscale space is then constructed by subtracting the corrected space $\mathcal{Q}V_H$ from V_H, i.e., $V_{\mathrm{ms}} := V_H - \mathcal{Q}V_H$. The solution space has thus been decomposed as $V = V_{\mathrm{ms}} \oplus V_{\mathrm{f}}$, where the elements of V_{ms} and V_{f} are orthogonal with respect to $(K\cdot,\cdot)$. In similarity to the standard LOD method, the space V^{ms} can be used to compute coarse-scale approximations to (4.3.1) that remain accurate. However, creating V_{ms} necessitates solving the global corrector system (4.3.5) for each basis function λ_i, $i = 1, \ldots, m_0$, which quickly becomes computationally demanding for large systems. Fortunately, in [17], it was proven that a corrected basis function, just like for the standard LOD, satisfies an exponential decay away from its corresponding support. For an illustration of a modified basis function, and its decay, see Figure 4.9. Due to the decay, the localization procedure from Section 2.1 can be repeated to define the localized counterpart to V_{ms}, denoted $V_{\mathrm{ms},k}$, where k is the localization parameter determining the size of the grid patches (recall Figure 3.2).

Before stating the final method, the wave equation (4.3.1) further requires a discretization of the temporal domain, which follows in a more traditional fashion. In similarity to Section 2.2, we consider the uniform partition $0 =: t_0 < t_1 < \ldots < t_N := T$ of $[0, T]$ with time step $\tau = t_n - t_{n-1}$. We deploy the scheme used for the standard wave equation in (2.2.9). In total, the fully

discretized LOD based method becomes: find $u^n_{\mathrm{ms},k} \in V_{\mathrm{ms},k}$ for $n = 2, \dots, N$ such that

$$(M\partial_t\bar{\partial}_t u^n_{\mathrm{ms},k}, v) + (K\tfrac{1}{2}(u^{n+1/2}_{\mathrm{ms},k} + u^{n-1/2}_{\mathrm{ms},k}), v) = (f^n, v), \tag{4.3.6}$$

for all $v \in V_{\mathrm{ms},k}$ with initial values $u^0_{\mathrm{ms},k}, u^1_{\mathrm{ms},k} \in V_{\mathrm{ms},k}$.

Theoretical results

For the method (4.3.6), it holds that the energy is conserved through all time steps. Indeed, if $f \equiv 0$, then

$$\left|\partial_t u^n_{\mathrm{ms},k}\right|^2_M + \left|u^{n+1/2}_{\mathrm{ms},k}\right|^2_K = \left|\partial_t u^0_{\mathrm{ms},k}\right|^2_M + \left|u^{1/2}_{\mathrm{ms},k}\right|^2_K,$$

holds for all $n \geq 0$, which can be shown by following the proof of [42, Lemma 13.2] with $V_{\mathrm{ms},k}$ as the test function space. In Paper III, an a priori error analysis is presented for the scheme (4.3.6), where convergence of optimal order is shown. The analysis borrows elements from the LOD theory for the continuous wave equation (see [2]), the discrete LOD theory for stationary matrix systems (see [17]), and standard finite elements results for hyperbolic equations (see, e.g., [42]). One part is also dedicated to stability analysis of operators in the norms based on the matrices M and K.

We state the main result for the proposed method (4.3.6), and refer to Paper III for the details on the full analysis. In the theorem statement, we use the operator R^{ms}_k, which denotes the Ritz-projection with respect to $(K\cdot,\cdot)$ onto V^{ms}, i.e., for any $v \in V$ it holds that $(KR^{\mathrm{ms}}_k v, w) = (Kv, w)$ for all $w \in V^{\mathrm{ms}}$. We moreover state a requirement of so-called *well-prepared data*. This assumption deals with the high order derivatives on the initial values which appear in a priori analysis of wave equations. See, e.g., [2] or Paper III for further discussion on well-prepared data.

Theorem 4.3.3. *Let the localization parameter be chosen such that $k \sim \log(1/H)$, and assume the initial values, $u^0_{\mathrm{ms},k}, u^1_{\mathrm{ms},k}$, satisfy*

$$\left|\partial_t u^0_{\mathrm{ms},k} - R^{\mathrm{ms}}_k u(t_0)\right|_M + \left|u^{1/2}_{\mathrm{ms},k} - R^{\mathrm{ms}}_k u(t_{1/2})\right|_K \leq C(H + \tau^2).$$

Moreover, the data is assumed to be well-prepared and compatible of order 3. Then, the error between the multiscale approximation and the reference solution satisfies

$$\left|\partial_t u^n_{\mathrm{ms},k} - D_t u(t_{n+1/2})\right|_M + \left|u^{n+1/2}_{\mathrm{ms},k} - u(t_{n+1/2})\right|_K \leq C(H + \tau^2),$$

where the constant C is independent of the complex features inherited by the network.

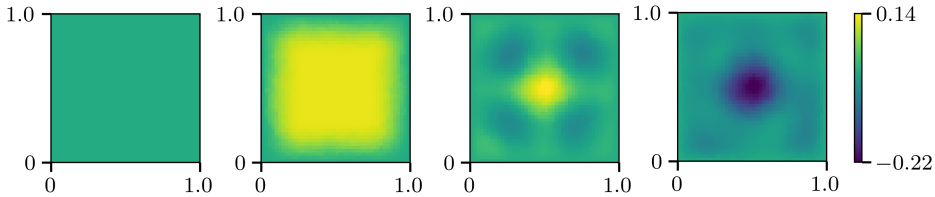

Figure 4.10: The reference solution u^n of (4.3.7) plotted at time steps $t = 0, 2/3, 4/3, 2$.

Numerical example

We conclude the section on wave propagation on spatial networks by a numerical example. For the model problem, we use the matrix K defined in (4.3.3), and consider the scalar valued problem

$$\begin{cases} MD_t^2 u + Ku = M\left(\sin(2\pi t)\cdot 1\right),\ t \in [0,2] \\ u = 0,\ x \in \partial D, \\ u(0) = 0,\ D_t u(0) = 0, \end{cases} \tag{4.3.7}$$

where $1 \in V$. We measure the error by comparing with a reference solution u^n computed on the full network discretization. For both the reference solution and the LOD approximation, the temporal domain is discretized with a time step $\tau = 2 \cdot 10^{-3}$. The LOD approximation $u^n_{\mathrm{ms},k}$ is computed with coarse mesh sizes H^{-i}, $i = 2, \ldots, 5$ with localization parameter $k = \log_2(1/H)$. In Figure 4.10, the reference solution is displayed at four different points on time, and Figure 4.11 shows the optimal order convergence in both M-norm and K-norm.

Remark 4.3.4. The numerical example is set in a scalar-valued setting. In practice, it is more interesting to consider the modeling of elastic waves, which corresponds to the vector-valued case. However, as thoroughly done in [17, 23], and remarked in Paper III, it is possible to extend the theory to the vector-valued setting. In Paper III, a final numerical example is provided where an elastic wave equation is considered, for which it is numerically verified that the optimal order convergence is achieved for such cases as well.

4.4 Parabolic SPDE with additive noise

The final part of this thesis considers the LOD framework applied to stochastic partial differential equations. As model problem, we use the parabolic SPDE

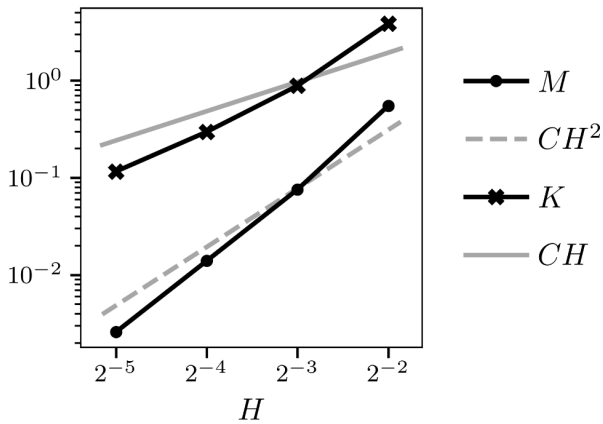

Figure 4.11: Convergence of the LOD approximation $u^n_{\mathrm{ms},k}$ in M-norm and K-norm.

with additive noise

$$\begin{aligned} \mathrm{d}X + \Lambda X \ \mathrm{d}t &= G\,\mathrm{d}W, && \text{in } D \times (0,T], \\ X &= 0, && \text{on } \partial D \times (0,T], \\ X(\cdot,0) &= X_0, && \text{in } D. \end{aligned} \tag{4.4.1}$$

where X is a V-valued random process for some separable Hilbert space V, D is a polygonal (or polyhedral) domain in $\mathbb{R}^d$, $d = 2, 3$, $\Lambda := -\nabla \cdot A\nabla$ is an operator with (rapidly oscillating) diffusion $A = A(x)$, and X_0 is the (possibly stochastic) initial value. The noise W is an U-valued Q-Wiener process defined on the filtered probability space $(\Omega, \mathcal{F}, \mathbb{P}, \{\mathcal{F}_t\}_{t\geq 0})$, and $G \in L(U;V)$ maps the noise between the separable Hilbert spaces U and V.

Simulation of SPDEs is of importance to a wide range of real-life applications. This includes models in physics, chemistry, biology and mathematical finance (see, e.g., [46] for more applications). In particular, the system (4.4.1) with multiscale effects appears, for instance, when modeling heat flow in an inhomogeneous (e.g., composite) material with uncertainties in measurements of the source term. The theory on parabolic SPDEs is by now well-established. For results on existence and uniqueness, regularity, asymptotic behavior, and further properties of the solution, we refer to [15, 38].

Notes on the FEM approach

From a computational perspective, strong convergence has been derived for the finite element method in [66, 67] (with extension to the semi-linear case in [38]). However, as remarked in Section 2.3, the mesh size must be small enough to resolve the oscillations in the diffusion in order to achieve the derived order of convergence. To avoid this requirement, we apply the LOD framework to (4.4.1) and derive a priori optimal order convergence rate independent of the variations in A. For the details of the method and the corresponding analysis, we refer to the work in Paper IV.

From Section 2.3, we recall the backward Euler–Galerkin scheme (2.3.6), for which the solution can be expressed by

$$X_h^n = E_{\tau,h}^n P_h X_0 + \sum_{j=1}^{n} \int_{t_{j-1}}^{t_j} E_{\tau,h}^{n-j+1} P_h G \, \mathrm{d}W(s). \tag{4.4.2}$$

In [38], the author derives an a priori error bound for the strong error of the form (2.3.8). However, the analysis makes use of elliptic regularity estimates, both in terms of estimating $\|X\|_{H^2(D)}$, as well as implicitly by properties of the heat semigroup $E(t)$ generated by the Laplacian. In our case, where $\Lambda = -\nabla \cdot A\nabla$ and A contains rapid variations, such estimates are prohibited in the analysis since the constant depends on the variations in A.

The LOD method

We consider the LOD method corresponding to (4.4.1). For this purpose, let $V_{\mathrm{ms},k}$ be the localized multiscale space constructed in complete analogy with Section 3.1. The goal is to express a similar backward Euler–Galerkin scheme as (2.3.6), but posed on $V_{\mathrm{ms},k}$. For this purpose, let $P_k^{\mathrm{ms}} : V_h \to V_{\mathrm{ms},k}$ be the $L_2(D)$-projection onto $V_{\mathrm{ms},k}$, i.e., for any $v \in V_h$, it holds that

$$(P_k^{\mathrm{ms}} v, w) = (v, w),$$

for all $w \in V_h$, and define the composed operator $P_{k,h}^{\mathrm{ms}} = P_k^{\mathrm{ms}} \circ P_h$, where P_h is the standard $L_2(D)$-projection onto V_h defined in (2.3.5). It holds that such a projection is well-defined, since one can expand the functions in the basis $\{\lambda_x - \mathcal{Q}_{\mathrm{f},k}\lambda_x\}_{x\in\mathcal{N}}$ that spans $V_{\mathrm{ms},k}$, which in turn yields a symmetric positive-definite matrix system. On $V_{\mathrm{ms},k}$, we moreover define the localized

diffusion operator $\Lambda_k^{\mathrm{ms}} : V_{\mathrm{ms},k} \to V_{\mathrm{ms},k}$ by the relation

$$(\Lambda_k^{\mathrm{ms}} v, w) = a(v, w),$$

for all $v, w \in V_{\mathrm{ms},k}$. The proposed method states: find $X_{\mathrm{ms},k}^n \in V_{\mathrm{ms},k}$ for $n = 1, \dots, N$ with initial value $P_{k,h}^{\mathrm{ms}} X_0$, such that

$$X_{\mathrm{ms},k}^n - X_{\mathrm{ms},k}^{n-1} + \tau \Lambda_k^{\mathrm{ms}} X_{\mathrm{ms},k}^n = \int_{t_{n-1}}^{t_n} P_{k,h}^{\mathrm{ms}} G \, \mathrm{d}W(s). \tag{4.4.3}$$

In similarity to how the solution to the standard backward Euler–Galerkin scheme can be written on the form (4.4.2), we have that (4.4.3) satisfies

$$X_{\mathrm{ms},k}^n = E_{\tau,k,n}^{\mathrm{ms}} P_{k,h}^{\mathrm{ms}} X_0 + \sum_{j=1}^{n} \int_{t_{j-1}}^{t_j} E_{\tau,k,n-j+1}^{\mathrm{ms}} P_{k,h}^{\mathrm{ms}} G \, \mathrm{d}W(s), \tag{4.4.4}$$

where we have defined $E_{\tau,k,n}^{\mathrm{ms}} := ((I + \tau \Lambda_k^{\mathrm{ms}})^{-1})^n$.

Error analysis

The goal of Paper IV is to derive an a priori error bound for the strong error, in similarity to (2.3.8), but independent of the scale ε at which the diffusion oscillates. The analysis is mainly based on a combination of the LOD theory for deterministic parabolic problems (see [50]), with modified results from finite element theory for SPDEs. The modifications include, in particular, error bounds between the operators $E_{\tau,h}^n$ and $E_{\tau,k,n}^{\mathrm{ms}}$ independent of the scale ε. In total, we find the following theorem for the strong error between the mild reference solution X_h^n from (4.4.2) computed on the fine scale and the LOD approximation $X_{\mathrm{ms},k}^n$. For the specific details of the analysis, we refer to the work in Paper IV.

Theorem 4.4.1. *Let X_h^n be the finite element reference solution of* (4.4.1)*, given by the formula* (4.4.2)*, and let $X_{\mathrm{ms},k}^n$ be the LOD approximation from* (4.4.4)*. Then, for $\mu \in [1, 2]$, the error satisfies*

$$\|X_h^n - X_{\mathrm{ms},k}^n\|_{L_2(\Omega; L_2(D))} \leq C H^{\mu},$$

where the constant is independent of the variations in the diffusion A.

The convergence order μ in the theorem statement is a parameter that depends on the regularity of the initial value and the covariance operator Q. We emphasize that under sufficient regularity, it holds that the solution converges

strongly with optimal order, and refer to the analysis in Paper IV for the details.

Monte-Carlo estimation

As remarked in Section 2.3, it is often interesting to analyze the expectation of the solution to (4.4.1), or more generally the expectation of some Lipschitz function $g : L_2(D) \to \mathcal{B}$. We seek to approximate the quantity $\mathbb{E}[g(X(t_n))]$ by combining the LOD method with the Monte-Carlo approach from Section 2.3. That is, the full LOD Monte-Carlo estimator is given by

$$\mathbb{E}[g(X^n_{\mathrm{ms},k})] \approx E_M[g(X^n_{\mathrm{ms},k})] := \frac{1}{M}\sum_{m=1}^{M} g(X^{n,m}_{\mathrm{ms},k}),$$

where $\{X^{n,m}_{\mathrm{ms},k}\}_{m=1}^{M}$ are independent and identically distributed random samples with the same distribution as $X^n_{\mathrm{ms},k}$. By repeating the arguments from Section 2.3, and applying the strong convergence rate from Theorem 4.4.1, the full weak error satisfies

$$\|\mathbb{E}[g(X(t_n))] - E_M[g(X^n_{\mathrm{ms},k})]\|_{L_2(\Omega;L_2(D))} \leq C\Big(\tau + H^2 + \frac{1}{\sqrt{M}}\Big), \quad (4.4.5)$$

where the constant is independent of the variations in the diffusion A.

We quickly note the computational benefits that the LOD method brings to the table. The key difference between this estimate and the estimate (2.3.12) for the finite element approach, is the absence of the ε-dependence in the spatial term. That is, we achieve convergence immediately without the requirement to resolve ε. For the Monte-Carlo estimation, this is implies that each simulation $X^{n,m}_{\mathrm{ms},k}$ is computed on a coarse grid of mesh size H, in contrast to the finite element case (see Section 2.3), where the simulations require a mesh size $h < \varepsilon$.

Multilevel Monte-Carlo

The LOD Monte-Carlo estimator manages to achieve quadratic convergence rate for the weak error, independent of ε. However, this follows under the assumption that the number of samples is proportional to the coarse mesh size as $M \sim H^{-4}$, which in turn is computationally demanding. In order to reduce the complexity, we combine the LOD method with the multilevel Monte-Carlo method, presented in Section 2.3. For this purpose, let $X^n_{\mathrm{ms},k,j}$ denote the LOD approximation from the multiscale space $V_{\mathrm{ms},k}$ based on the discretization $\mathcal{T}_{H_j}$.

By replacing the standard finite element solution by the LOD approximation in (2.3.13), we have the LOD multilevel Monte-Carlo estimator

$$E^J[g(X^{n,m}_{\mathrm{ms},k,J})] := E_{M_0}[g(X^{n,m}_{\mathrm{ms},k,0})] + \sum_{j=1}^{J} E_{M_j}[g(X^{n,m}_{\mathrm{ms},k,j}) - g(X^{n,m}_{\mathrm{ms},k,j-1})].$$

We combine the arguments from Section 2.3, with the convergence results for the LOD approximation. This yields the error estimate

$$\|\mathbb{E}[g(X(t_n))] - E^J[g(X^n_{\mathrm{ms},k,J})]\|_{L_2(\Omega;\mathcal{B})} \leq C\Big(\tau + H_J^2 + \frac{1}{\sqrt{M_0}} + \sum_{j=1}^{J} \frac{H_j^2}{\sqrt{M_j}}\Big).$$

That is, the similar estimate as for the finite element holds, but independent of the scale ε. If we furthermore choose the sample sizes as $M_0 = \gamma H_J^{-4}$ and $M_j = M_0 H_j^4 \cdot 2^{2\delta j}$ for some proportionality constant γ and $\delta > 0$, we get

$$\|\mathbb{E}[g(X(t_n))] - E^J[g(X^n_{\mathrm{ms},k,J})]\|_{L_2(\Omega;\mathcal{B})} \leq C(\tau + H_J^2), \tag{4.4.6}$$

where the constant depends on, e.g., the contrast in the diffusion A and the parameters γ and δ, but is independent of the variations in A.

Numerical examples

We conclude the section on SPDEs with two numerical examples. At first, we illustrate the strong convergence stated in Theorem 4.4.1. The second example shows the weak convergence, where the expectation of the LOD approximation is computed using a standard Monte-Carlo estimator and a multilevel Monte-Carlo estimator, respectively. Furthermore, an illustration of the computational time required for the different methods is included, which highlights the efficiency of the LOD method in the context of SPDEs.

As model problem for the numerical examples, we consider the system (4.4.1) with an additional source term f added in the right-hand side, i.e.,

$$\mathrm{d}X(t) + \Lambda X(t)\,\mathrm{d}t = f(t)\,\mathrm{d}t + G\,\mathrm{d}W(t). \tag{4.4.7}$$

By adding extra source data to the system, the amplitude of the solution will not vanish as rapidly. Consequently, we can include higher contrast in the diffusion, which in turn yields a more interesting solution.

Remark 4.4.2. Throughout this section, we have considered the equation (4.4.7) with $f \equiv 0$. However, by linearity, one can decompose the solution as $X =$

$X_1 + X_2$, where X_1 satisfies (4.4.7) with $f \equiv 0$, and X_2 is the solution with zero noise, i.e., the deterministic case where $W \equiv 0$. Therefore, the error can be split as

$$\|X_h^n - X_{\mathrm{ms},\ell}^n\|_{L_2(\Omega;L_2)} \leq \|X_{h,1}^n - X_{\mathrm{ms},\ell,1}^n\|_{L_2(\Omega;L_2)} + \|X_{h,2}^n - X_{\mathrm{ms},\ell,2}^n\|_{L_2(\Omega;L_2)},$$

where the analysis for the second term follows immediately from the deterministic analysis, made in [50].

For the examples, we use the unit square domain $D = [0,1] \times [0,1]$. The diffusion is generated as a piecewise constant function whose values vary in the interval $[0.01, 10]$ at the scale $\varepsilon = 2^{-6}$. The fine discretization is performed with fine mesh width $h = 2^{-8}$, such that it resolves the variations in the diffusion. The temporal domain is discretized with time step $\tau = 0.01$, as initial data we set $X_0(x,y) = \sin(\pi x)\sin(\pi y)$ and the source is chosen as $f \equiv 5$.

For the noise, recall the Karhunen–Loève expansion of W from (2.3.1). In numerical simulations, this expansion is truncated up to a parameter κ (set to $\kappa \sim h^{-1}$ in our examples). That is, we use the noise approximation

$$W^\kappa(x,y,t) = \sum_{m=1}^{\kappa}\sum_{n=1}^{\kappa} \sqrt{\lambda_{m,n}}\beta_{m,n}(t)e_{m,n}(x,y),$$

where $\{\beta_{m,n}(t)\}_{m,n}$ are mutually independent, real-valued Brownian motions, and $e_{m,n}$ are the eigenvalues to the covariance operator Q with corresponding eigenvalues $\{\lambda_{m,n}\}$. The operator Q in the numerical examples is defined through the choice of $e_{m,n}$ and $\lambda_{m,n}$, where $\lambda_{m,n}$ determines the amplitude of the noise, and consequently the variance of the solution. The eigenfunctions are set to $e_{m,n} = \sin(n\pi x)\sin(m\pi y)$, and we let $\lambda_{m,n} = \Theta(m^{2.01} + n^{2.01})^{-1}$, where Θ determines the amplitude of the noise, and consequently the variance and smoothness of the solution.

The strong error between the reference solution X_h^n and the LOD approximation $X_{\mathrm{ms},k}^n$ is computed for coarse grid sizes $H = 2^{-i}$, $i = 1, \ldots, 6$, with localization parameter $k = \log_2(1/H)$ and noise parameter $\Theta = 1$. The error is compared in $L_2(\Omega; L_2(D))$-norm at the final time $T = 0.5$. In Figure 4.12, the reference solution and the corresponding noise at the final time is shown. Since the norm is a random variable, we estimate it by a Monte-Carlo estimator with 100 samples, i.e., $\|\cdot\|_{L_2(\Omega;L_2(D))} \approx E_{100}[\|\cdot\|]$. We also include the FEM approximation for coarse grid sizes as comparison, as well as an $\mathcal{O}(H^2)$-reference line indicating the convergence rate from Theorem 4.4.1. The convergence is displayed in Figure 4.13, where it is seen how the LOD approximation converges

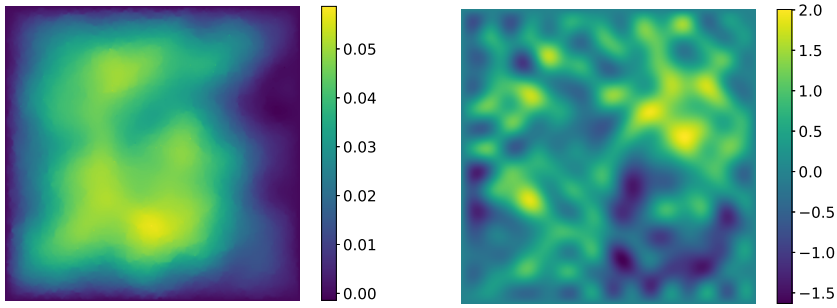

(a) X_h^N. **(b)** $W^\kappa(x, y, t_N)$.

Figure 4.12: The reference solution X_h^N and the truncated noise $W^\kappa(x, y, t_N)$, plotted at final time $t_N = 0.5$.

with second order, while the FEM error remains constant for all grid sizes.

For the weak error, we analyze the convergence of the expectation of the solution, i.e., the error between $\mathbb{E}[X_h^n]$ and its corresponding LOD approximation. In order to compare the performance between the standard Monte-Carlo and the multilevel Monte-Carlo estimators, we fix $H = H_J$ for the standard Monte-Carlo estimation and denote by $X^n_{\mathrm{ms},k,J}$ the LOD approximation on the coarse grid with mesh size H_J. We decrease the noise amplitude parameter to $\Theta = 5^{-2}$ such that the variance is reduced. This is done to lower the requirement on the number of samples necessary for the Monte-Carlo estimation. Moreover, note that the expectation of the solution to (4.4.7) satisfies a deterministic equation (since the noise has zero mean). Consequently, the reference solution $\mathbb{E}[X_h^n]$ can be computed without any Monte-Carlo estimation.

It was previously shown that the weak error consists of a deterministic part and a statistical part, respectively. As an example, the estimator $E_M[X^N_{\mathrm{ms},\ell,J}]$ is computed for $H_J = 2^{-(J+1)}$, $J = 0, \dots, 5$, with $M = 10000$ samples on each mesh size, and the total error is plotted as a function of M. The result is depicted in Figure 4.14, where horizontal lines are included that indicate the size of the deterministic error for each coarse mesh size. In the figure, we see that after 10000 samples the statistical error has vanished for $H_J = 2^{-1}, \dots, 2^{-4}$, while it still remains for $H_J = 2^{-5}, 2^{-6}$. As earlier pointed out, the deterministic and statistical errors are balanced by choosing the samples of the Monte-Carlo estimator proportional to the mesh size as $M_J \sim H_J^{-4}$.

Next, we compute an estimation of $\mathbb{E}[X^N_{\mathrm{ms},k,J}]$ using standard Monte-Carlo estimation (LOD-MC) and multilevel Monte-Carlo estimation (LOD-MLMC),

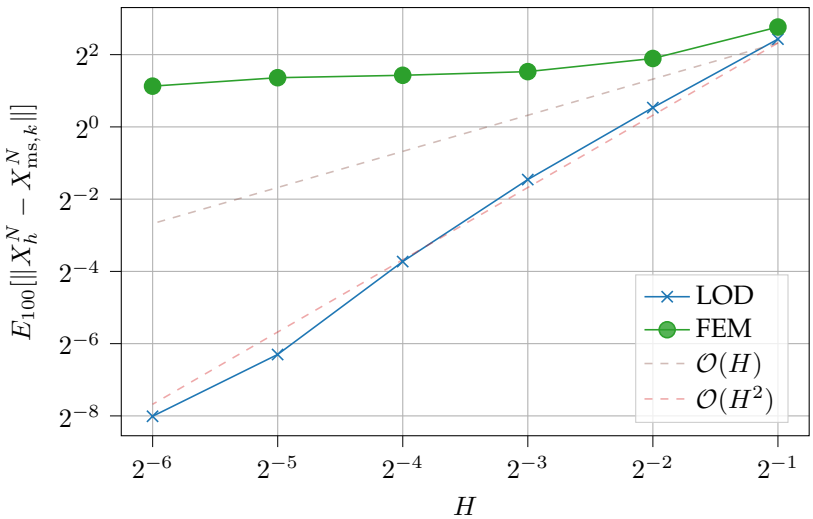

Figure 4.13: The strong error at final time $t_N = 0.5$ between the multiscale approximation $X_{\mathrm{ms},k}^N$ and the reference solution X_h^N computed on the fine grid. The norm is estimated as $\|\cdot\|_{L_2(\Omega;L_2(D))} \approx E_{100}[\|\cdot\|]$, i.e., by a Monte-Carlo estimator with $M = 100$ samples.

respectively. For all estimators, we set $\gamma = 0.01$ as a scaling parameter for the number of samples. The standard Monte-Carlo estimator $E_{M_J}[X_{\mathrm{ms},k,J}^n]$ is evaluated with $M_J = \gamma H_J^{-4}$ number of samples. This is done for coarse mesh sizes $H_J = 2^{-(J+1)}$, $J = 0, \dots, 4$. For the multilevel Monte-Carlo estimator $E^J[X_{\mathrm{ms},k,J}^n]$ we set $M_0 = \gamma H_J^{-4}$ and let $M_j = M_0 H_j^4 \cdot 2^{2\delta j}$ for $j = 1, \dots, J$, with $\delta = 1$. The estimator is evaluated for mesh sizes $H_J = 2^{-(J+1)}$, $J = 0, \dots, 5$. In Figure 4.15, the convergence of the weak error for both estimators is illustrated. For comparison, the Monte-Carlo estimation of the finite element solution based on the coarse grid (FEM-MC) is included, i.e., $E_{M_J}[X_{H_J}^N]$ with $M_J = \gamma H_J^{-4}$. We note that both the standard and multilevel Monte-Carlo estimators of the LOD solution converge with quadratic rate, as predicted in (4.4.5) and (4.4.6). In contrast, we see that the finite element solution evaluated on the coarse mesh does not reach the region of convergence, since the mesh is unable to resolve the variations in the diffusion.

We conclude with a note on the computational complexity of computing $\mathbb{E}[X_{\mathrm{ms},k,J}^N]$ using the LOD-MC and LOD-MLMC estimators, respectively. We compare these methods with the Monte-Carlo estimation of a finite element solution computed on the fine grid with mesh size h. Note that, although the LOD-MC and FEM-MC methods require the same number of samples, i.e.,

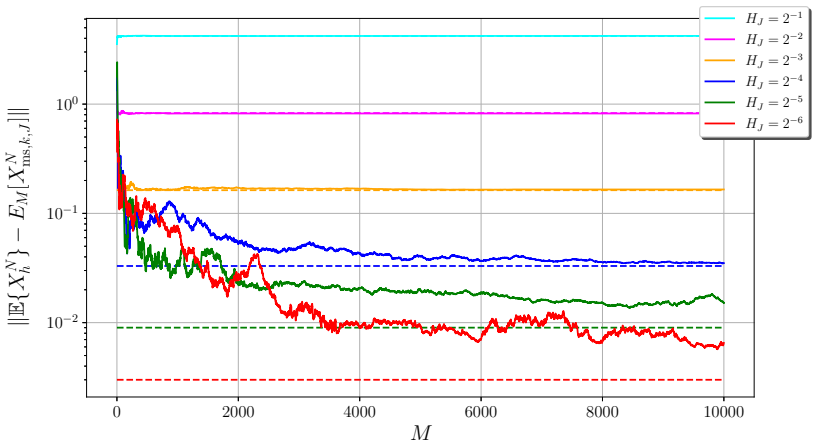

Figure 4.14: The error for the Monte-Carlo estimator of the LOD approximation, as function of the number of samples M. The horizontal lines indicate the discretization error for each coarse mesh size H, respectively.

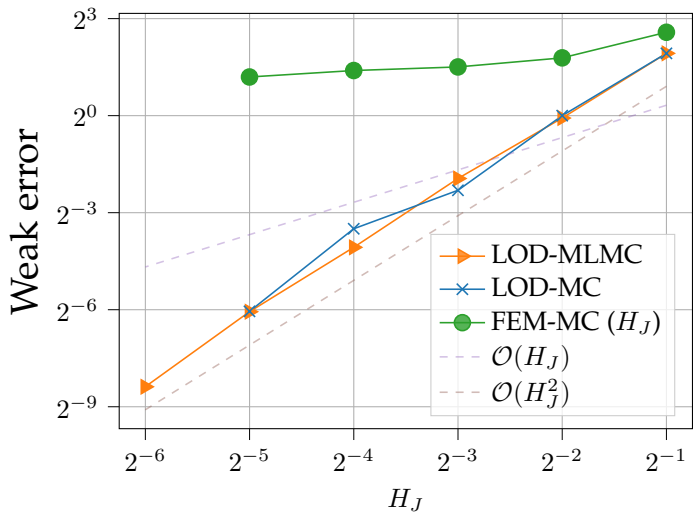

Figure 4.15: The weak error as function of the coarse mesh size H_J. For LOD-MC and FEM-MC, the number of samples are chosen as $M_J = \gamma H_J^{-4}$ with $\gamma = 0.01$. In the multilevel estimation, the samples are set to $M_0 = \gamma H_J^{-4}$ and $M_j = M_0 H_j^4 \cdot 2^{2\delta j}$ for $j = 1, \ldots, J$ with $\delta = 1$.

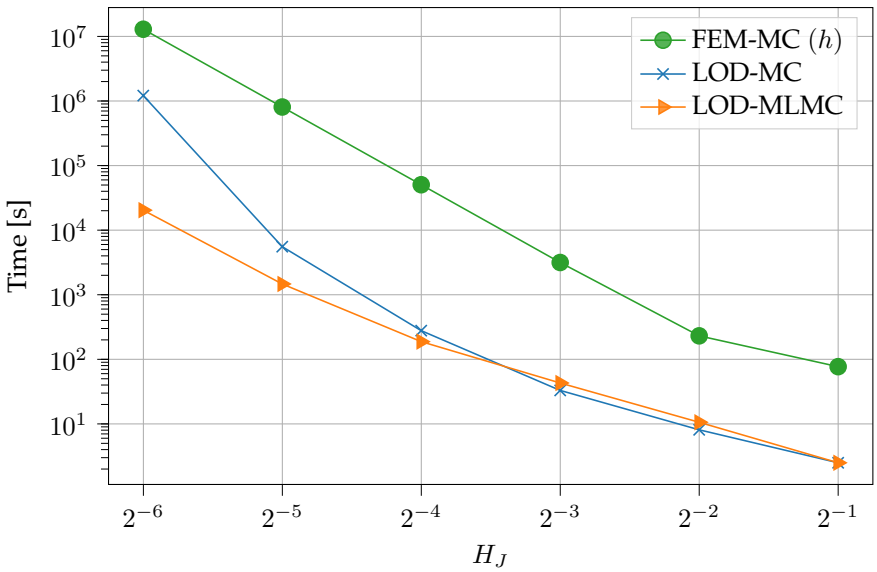

Figure 4.16: The running time for the different methods of estimating the quantity $\mathbb{E}[X^N_{\mathrm{ms},k,J}]$. The samples for the FEM-MC and LOD-MC estimators are chosen as $M_J = \gamma H_J^{-4}$, and for the LOD-MLMC estimator the samples are set to $M_0 = \gamma H_J^{-4}$ and $M_j = M_0 H_j^4 \cdot 2^{2\delta j}$, with parameters $\gamma = 0.01$ and $\delta = 1$.

$M_J \sim H_J^{-4}$, the LOD-MC computes the samples on a coarse grid of mesh size H_J, while the FEM-MC samples are evaluated on a fine mesh. An additional advantage is gained by applying the LOD-MLMC estimator, since the number of samples on the finest coarse grid is always limited to $M_J \sim 2^{2\delta J}$, independent of the total number of samples. To emphasize the computational gain, we compare the total time required for the weak error simulations in each case. The times are logged for the coarse mesh sizes $H_J = 2^{-1}, \dots, 2^{-6}$, where the number of samples for the standard Monte-Carlo estimation is $M_J = \gamma H_J^{-4}$ with $\gamma = 0.01$ and in the multilevel case we set $M_0 = \gamma H_J^{-4}$ and $M_j = M_0 H_j^4 \cdot 2^{2\delta j}$, $j = 1, \dots, J$, with $\delta = 1$. The total computational time as a function of the coarse mesh size H_J is plotted for each method, and illustrated in Figure 4.16. We note that the computational time for FEM-MC is magnitudes larger than each LOD-based method. The contrast between LOD-MC and LOD-MLMC is small for coarse mesh sizes, but as H_J decreases the LOD-MLMC method shows significant advantage.

5 Summary of papers

Paper I. In Paper I we propose and analyze the GFEM in (4.1.5)-(4.1.6), based on the LOD method, for strongly damped wave equations with rapidly varying data. The method is designed to handle independent variations in both the damping coefficient and wave propagation speed respectively. It does so by correcting for the damping in the transient phase, where it is as most effective, and automatically transitions into correcting for the wave propagation speed in the steady state phase, where the damping has vanished. Convergence of optimal order is proven for the ideal method, as well as the exponential decay of the basis corrector functions to justify the localization. Numerical examples are presented that confirm the theoretical findings.

Paper II. In Paper II we present the GFEM (4.2.3)-(4.2.4) extending the LOD framework to parabolic equations where the diffusion is highly oscillating in both time and space. The method computes a coarse-scale representation of the differential operator that contains information on the space-time variations in the diffusion. Once the coarse-scale representation is constructed, it can furthermore be reused to solve the system for multiple right-hand sides. Convergence of optimal order is proven for the ideal method. We illustrate the space-time decay of the basis correctors, which is necessary for the localized scheme. Numerical examples that illustrate the error convergence and the performance of the localized method are presented.

Paper III. In Paper III, the LOD method extended to spatial network models is applied to a discrete version of the linear wave equation, characterized by a symmetric positive-definite matrix K with high data variations. The method produces coarse-scale approximations by introducing an artificial grid and enrich it by K-dependent information computed on the high dimensional network model. The spatial discretization is combined with an energy conserving temporal scheme to compose the proposed method. A priori optimal order convergence is derived under the assumption of well-prepared initial data. The theoretical findings are confirmed by numerical examples for both

scalar-valued and elastic wave propagation.

Paper IV. In Paper IV, the LOD method is applied to a multiscale-type parabolic stochastic partial differential equation with additive noise. Optimal order convergence is derived for the strong error, which depends on the regularity of the data. Convergence of the weak error is analyzed by means of (multilevel) Monte-Carlo estimation. The theoretical results are verified by numerical examples and the computational efficiency of the LOD method is highlighted.

Bibliography

[1] A. Abdulle, W. E, B. Engquist, and E. Vanden-Eijnden. The heterogeneous multiscale method. *Acta Numer.*, 21:1–87, 2012.

[2] A. Abdulle and P. Henning. Localized orthogonal decomposition method for the wave equation with a continuum of scales. *Math. Comp.*, 86(304):549–587, 2017.

[3] R. Altmann, E. Chung, R. Maier, D. Peterseim, and S.-M. Pun. Computational multiscale methods for linear heterogeneous poroelasticity. *J. Comput. Math.*, 38(1):41–57, 2020.

[4] G. Avalos and I. Lasiecka. Optimal blowup rates for the minimal energy null control of the strongly damped abstract wave equation. *Ann. Sc. Norm. Super. Pisa Cl. Sci. (5)*, 2(3):601–616, 2003.

[5] J. Azevedo, C. Cuevas, and H. Soto. Qualitative theory for strongly damped wave equations. *Math. Method Appl. Sci.*, 40, 08 2017.

[6] I. Babuška, G. Caloz, and J. E. Osborn. Special finite element methods for a class of second order elliptic problems with rough coefficients. *SIAM J. Numer. Anal.*, 31(4):945–981, 1994.

[7] I. Babuška and J. E. Osborn. Generalized finite element methods: their performance and their relation to mixed methods. *SIAM J. Numer. Anal.*, 20(3):510–536, 1983.

[8] A. Barth and A. Lang. Multilevel Monte Carlo method with applications to stochastic partial differential equations. *Int. J. Comput. Math*, 89:2479 – 2498, 2012.

[9] A. Barth and T. Stüwe. Weak convergence of Galerkin approximations of stochastic partial differential equations driven by additive Lévy noise. *Math. Comput. Simul.*, 143:215–225, 2018. 10th IMACS Seminar on Monte Carlo Methods.

[10] K.-J. Bathe and M. M. I. Baig. On a composite implicit time integration procedure for nonlinear dynamics. *Comput. Struct.*, 83(31):2513–2524, 2005.

[11] K.-J. Bathe and G. Noh. Insight into an implicit time integration scheme for structural dynamics. *Comput. Struct.*, 98-99:1–6, 2012.

[12] E. Bonetti, E. Rocca, R. Scala, and G. Schimperna. On the strongly damped wave equation with constraint. *Commun. Partial Differ. Equ.*, 42(7):1042–1064, 2017.

[13] A. Carvalho and J. Cholewa. Local well posedness for strongly damped wave equations with critical nonlinearities. *Bull. Aust. Math. Soc.*, 66, 12 2002.

[14] C. Cuevas, C. Lizama, and H. Soto. Asymptotic periodicity for strongly damped wave equations. *Abstr. Appl. Anal.*, 2013, 09 2013.

[15] G. Da Prato and J. Zabczyk. *Stochastic Equations in Infinite Dimensions*. Encyclopedia of Mathematics and its Applications. Cambridge University Press, 2 edition, 2014.

[16] W. E and B. Engquist. The heterogeneous multiscale methods. *Commun. Math. Sci.*, 1(1):87–132, 2003.

[17] F. Edelvik, M. Görtz, F. Hellman, G. Kettil, and A. Målqvist. Numerical homogenization of spatial network models. *Preprint*, arXiv:2209.05808, 2022.

[18] Y. Efendiev, J. Galvis, and T. Y. Hou. Generalized multiscale finite element methods (GMsFEM). *J. Comput. Phys.*, 251:116–135, 2013.

[19] C. Engwer, P. Henning, A. Målqvist, and D. Peterseim. Efficient implementation of the localized orthogonal decomposition method. *Comput. Methods Appl. Mech. Eng.*, 350:123–153, 06 2019.

[20] F. Gazzola and M. Squassina. Global solutions and finite time blow up for damped semilinear wave equations. *Ann. Inst. H. Poincaré Anal. Non Linéaire*, 23(2):185–207, 2006.

[21] M. B. Giles. Multilevel Monte Carlo path simulation. *Oper. Res.*, 56(3):607–617, 2008.

[22] P. J. Graber and J. L. Shomberg. Attractors for strongly damped wave equations with nonlinear hyperbolic dynamic boundary conditions. *Nonlinearity*, 29(4):1171, 2016.

[23] M. Görtz, F. Hellman, and A. Målqvist. Iterative solution of spatial network models by subspace decomposition. *Preprint*, arXiv:2207.07488, 2022.

[24] M. Görtz, G. Kettil, A. Målqvist, M. Fredlund, K. Wester, and F. Edelvik. Network model for predicting structural properties of paper. *Nord. Pulp Pap. Res. J.*, 37(4):712–724, 2022.

[25] F. Hellman and A. Målqvist. Contrast independent localization of multiscale problems. *Multiscale Model. Simul.*, 15(4):1325–1355, 2017.

[26] P. Henning and A. Målqvist. Localized orthogonal decomposition techniques for boundary value problems. *SIAM J. Sci. Comput.*, 36(4):A1609–A1634, 2014.

[27] P. Henning, A. Målqvist, and D. Peterseim. A localized orthogonal decomposition method for semi-linear elliptic problems. *ESAIM Math. Model. Numer. Anal.*, 48(5):1331–1349, 2014.

[28] P. Henning and D. Peterseim. Oversampling for the multiscale finite element method. *Multiscale Model. Simul.*, 11(4):1149–1175, 2013.

[29] T. Y. Hou and X.-H. Wu. A multiscale finite element method for elliptic problems in composite materials and porous media. *J. Comput. Phys.*, 134(1):169–189, 1997.

[30] T. J. Hughes, G. R. Feijóo, L. Mazzei, and J.-B. Quincy. The variational multiscale method—a paradigm for computational mechanics. *Comput. Methods Appl. Mech. Eng.*, 166(1-2):3–24, 1998.

[31] D. Hào, N. Duc, and N. Thang. Backward semi-linear parabolic equations with time-dependent coefficients and local Lipschitz source. *Inverse Problems*, 34:055010, 05 2018.

[32] R. Ikehata. Decay estimates of solutions for the wave equations with strong damping terms in unbounded domains. *Math. Methods Appl. Sci.*, 24:659 – 670, 06 2001.

[33] V. Kalantarov and S. Zelik. A note on a strongly damped wave equation with fast growing nonlinearities. *J. Math. Phys.*, 01 2015.

[34] P. Kelly. *Solid Mechanics Part I: An Introduction to Solid Mechanics*. University of Auckland, 2019.

[35] G. Kettil, A. Målqvist, A. Mark, M. Fredlund, K. Wester, and F. Edelvik. Numerical upscaling of discrete network models. *BIT Numer. Math.*, 60:67–92, 03 2020.

[36] A. Khanmamedov. Strongly damped wave equation with exponential nonlinearities. *J. Math. Anal. Appl.*, 419(2):663 – 687, 2014.

[37] M. Kovács, S. Larsson, and F. Lindgren. Weak convergence of finite element approximations of linear stochastic evolution equations with additive noise. *BIT Numer. Math.*, 52:85–108, 2012.

[38] R. Kruse. *Strong and Weak Approximation of Semilinear Stochastic Evolution Equations*, volume 2093 of *Lecture Notes in Mathematics*. Springer Cham, 01 2014.

[39] A. Lang. A note on the importance of weak convergence rates for SPDE approximations in multilevel Monte Carlo schemes. In R. Cools and D. Nuyens, editors, *Monte Carlo and Quasi-Monte Carlo Methods*, pages 489–505, Cham, 2016. Springer International Publishing.

[40] M. G. Larson and A. Målqvist. Adaptive variational multiscale methods based on a posteriori error estimation: Duality techniques for elliptic problems. In *Multiscale Methods in Science and Engineering*, pages 181–193. Springer, 2005.

[41] M. G. Larson and A. Målqvist. Adaptive variational multiscale methods based on a posteriori error estimation: Energy norm estimates for elliptic problems. *Comput. Methods Appl. Mech. Eng.*, 196:2313–2324, 04 2007.

[42] S. Larsson and V. Thomée. *Partial Differential Equations with Numerical Methods*, volume 45. Springer-Verlag Berlin Heidelberg, 2003.

[43] S. Larsson, V. Thomée, and L. B. Wahlbin. Finite-element methods for a strongly damped wave equation. *IMA J. Numer. Anal.*, 11(1):115–142, 1991.

[44] Y. Lin, V. Thomée, and L. Wahlbin. *Ritz-Volterra projections to finite element spaces and applications to integro-differential and related equations*. Technical report (Cornell University. Mathematical Sciences Institute). Mathematical Sciences Institute, Cornell University, 1989.

[45] K. Lipnikov, G. Manzini, J. D. Moulton, and M. Shashkov. The mimetic finite difference method for elliptic and parabolic problems with a staggered discretization of diffusion coefficient. *J. Comput. Phys.*, 305:111–126, 2016.

[46] G. Lord, C. Powell, and T. Shardlow. *An Introduction to Computational Stochastic PDEs*. Cambridge Texts in Applied Mathematics. Cambridge University Press, 08 2014.

[47] R. Maier and D. Peterseim. Explicit computational wave propagation in micro-heterogeneous media. *BIT Numer. Math.*, 59(2):443–462, 2019.

[48] A. Målqvist. Multiscale methods for elliptic problems. *Multiscale Model. Simul.*, 9(3):1064–1086, 2011.

[49] A. Målqvist and A. Persson. A generalized finite element method for linear thermoelasticity. *ESAIM Math. Model. Numer. Anal.*, 51(4):1145–1171, 2017.

[50] A. Målqvist and A. Persson. Multiscale techniques for parabolic equations. *Numer. Math.*, 138(1):191–217, 2018.

[51] A. Målqvist and D. Peterseim. Localization of elliptic multiscale problems. *Math. Comp.*, 83(290):2583–2603, 2014.

[52] A. Målqvist and D. Peterseim. Generalized finite element methods for quadratic eigenvalue problems. *ESAIM Math. Model. Numer. Anal.*, 51(1):147–163, 2017.

[53] A. Målqvist and D. Peterseim. *Numerical homogenization by localized orthogonal decomposition*, volume 5 of *SIAM Spotlights*. Society for Industrial and Applied Mathematics (SIAM), Philadelphia, PA, 2020.

[54] A. Målqvist and B. Verfürth. An offline-online strategy for multiscale problems with random defects. *ESAIM Math. Model. Numer. Anal.*, 56(1):237–260, 2022.

[55] P. Massatt. Limiting behavior of strongly damped nonlinear wave equations. *J. Differ. Equ.*, 48:334–349, 06 1983.

[56] H. Owhadi. Multigrid with rough coefficients and multiresolution operator decomposition from hierarchical information games. *SIAM Rev.*, 59(1):99–149, 2017.

[57] H. Owhadi and C. Scovel. *Operator-adapted wavelets, fast solvers, and numerical homogenization*, volume 35 of *Cambridge Monographs on Applied and Computational Mathematics*. Cambridge University Press, Cambridge, 2019.

[58] S. Peszat and J. Zabczyk. *Stochastic Partial Differential Equations with Lévy Noise: An Evolution Equation Approach*. Encyclopedia of Mathematics and its Applications. Cambridge University Press, 2007.

[59] D. Peterseim. Variational multiscale stabilization and the exponential decay of fine-scale correctors. In *Building Bridges: Connections and Challenges in Modern Approaches to Numerical Partial Differential Equations*, volume 114 of *Lect. Notes Comput. Sci. Eng.*, pages 341–367. Springer, Cham, 2016.

[60] A. Quarteroni, A. Manzoni, and F. Negri. *Reduced Basis Methods for Partial Differential Equations: An Introduction*, volume 92 of *UNITEXT*. Springer Cham, 2015.

[61] M. Reed and B. Simon. *I: Functional Analysis*. Methods of Modern Mathematical Physics. Elsevier Science, 1981.

[62] H. Rui and H. Pan. Block-centered finite difference methods for parabolic equation with time-dependent coefficient. *Jpn. J. Ind. Appl. Math.*, 30:681–689, 2013.

[63] L. R. Scott and S. Zhang. Finite element interpolation of nonsmooth functions satisfying boundary conditions. *Math. Comput.*, 54(190):483–493, 1990.

[64] V. Thomée. *Galerkin Finite Element Methods for Parabolic Problems*, volume 25 of *Springer Series in Computational Mathematics*. Springer, 1997.

[65] K. Urban and A. T. Patera. An improved error bound for reduced basis approximation of linear parabolic problems. *Math. Comp.*, 83(288):1599–1615, 2014.

[66] Y. Yan. Semidiscrete Galerkin approximation for a linear stochastic parabolic partial differential equation driven by an additive noise. *BIT Numer. Math.*, 44:829–847, 12 2004.

[67] Y. Yan. Galerkin finite element methods for stochastic parabolic partial differential equations. *SIAM J. Numer. Anal.*, 43, 01 2005.

[68] S. Yousefi, D. Lesnic, and Z. Barikbin. Satisfier function in Ritz-Galerkin method for the identification of a time-dependent diffusivity. *J. Inverse Ill Posed Probl.*, 20, 12 2012.